EEG / ECoG

Ontology Droplet

Signal source

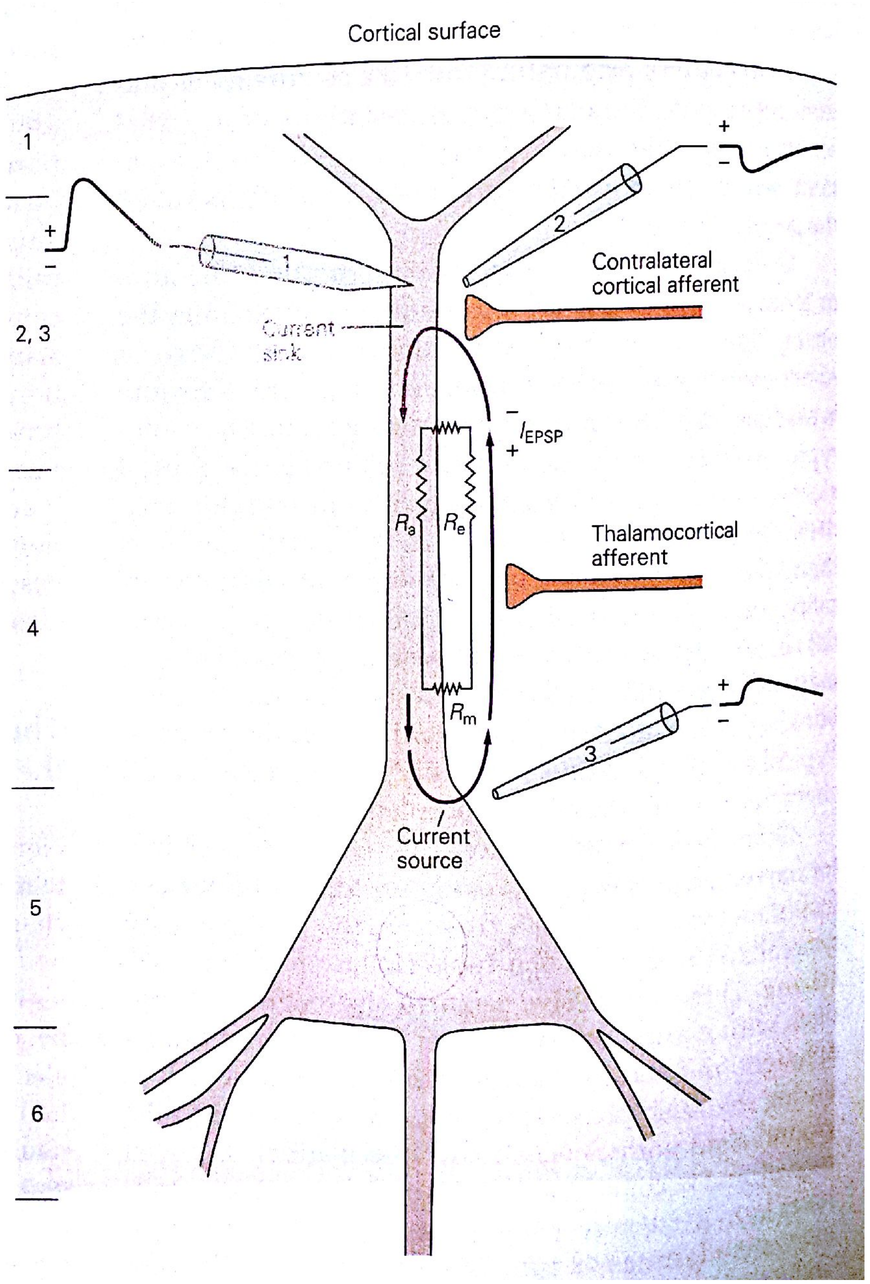

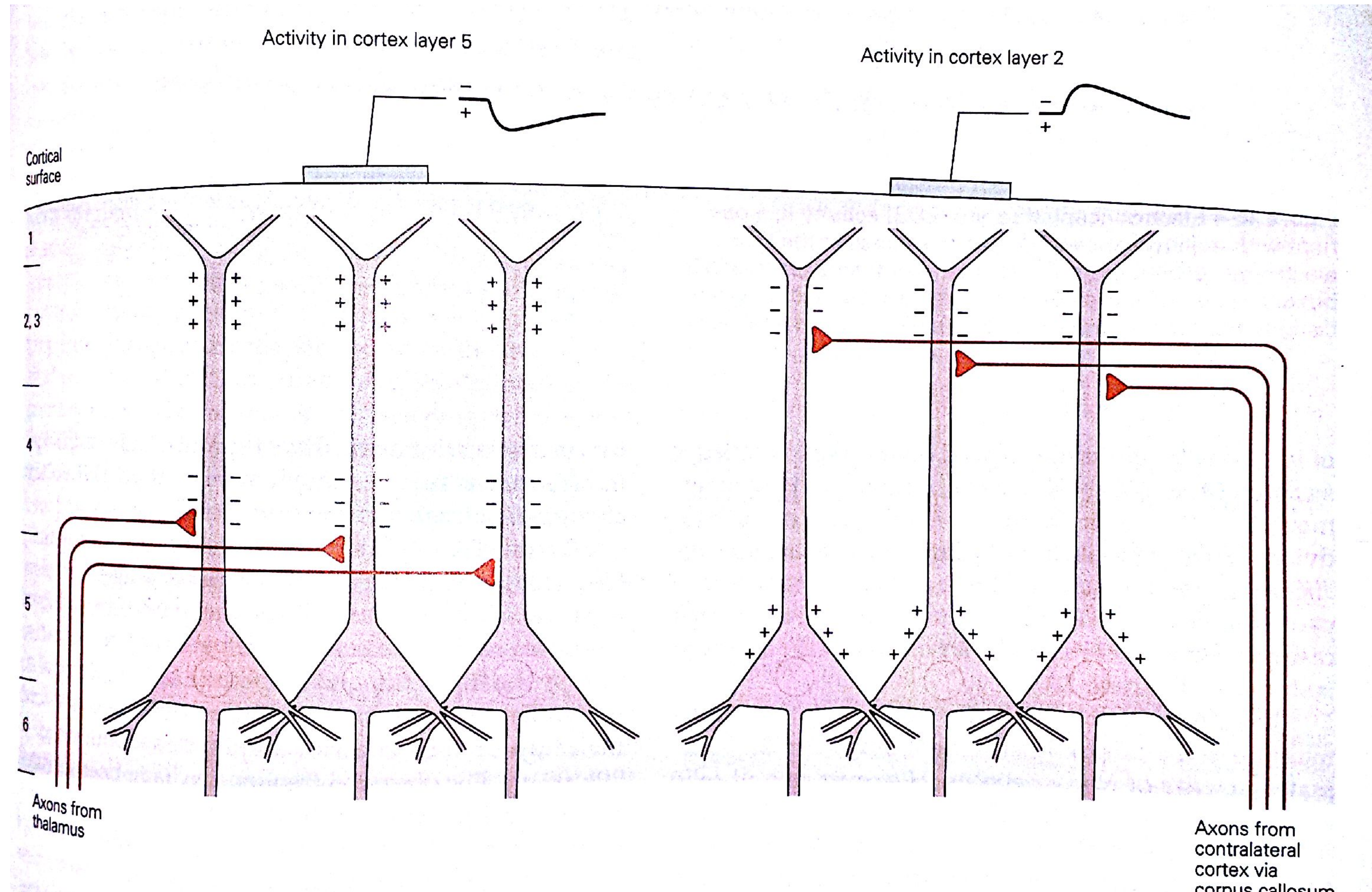

Figure 46-3 The polarity of the surface EEG depends on the location of the synaptic activity within the cortex. A thalamocortical excitatory input in layer 5 (**left**) causes a downward deflection at the surface EEG electrode because the EEG electrode is nearer to the source. In contrast, excitatory input from the contralateral hemisphere in layer 2 (**right**) causes an upward deflection because it is nearer to the sink.

Signal source

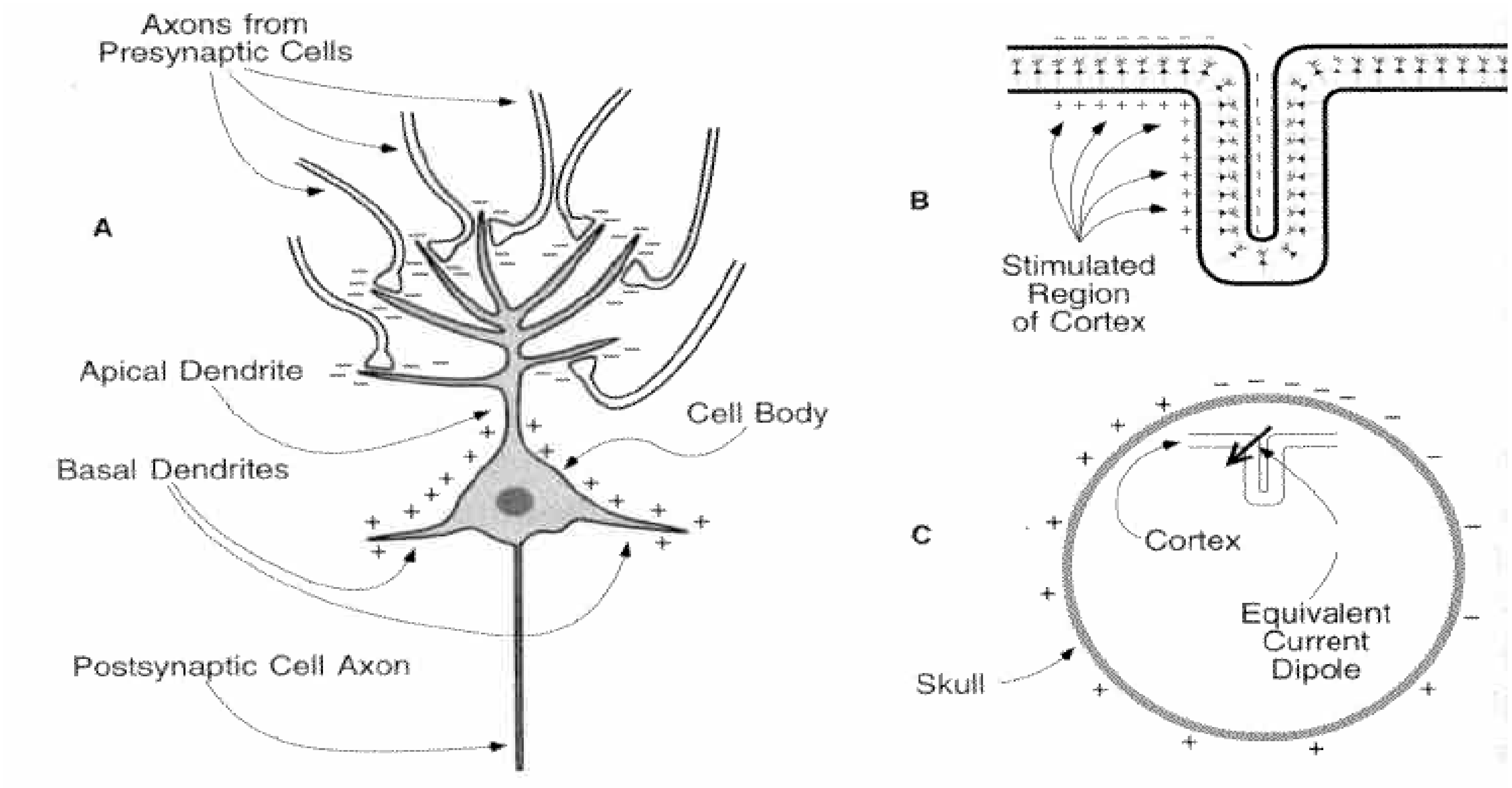

From Luck, S.J., (2005). *An Introduction to the Event-Related Potential Technique.* Cambridge, MA: MIT Press

Signal source

Inside the head:

Primary (postsynaptic, neuronal) current in red, secondary (volume) currents in green

Signal on the head surface:

Generated potential changes (= EEG maps/topographies). Blue: negativity Red: positivity

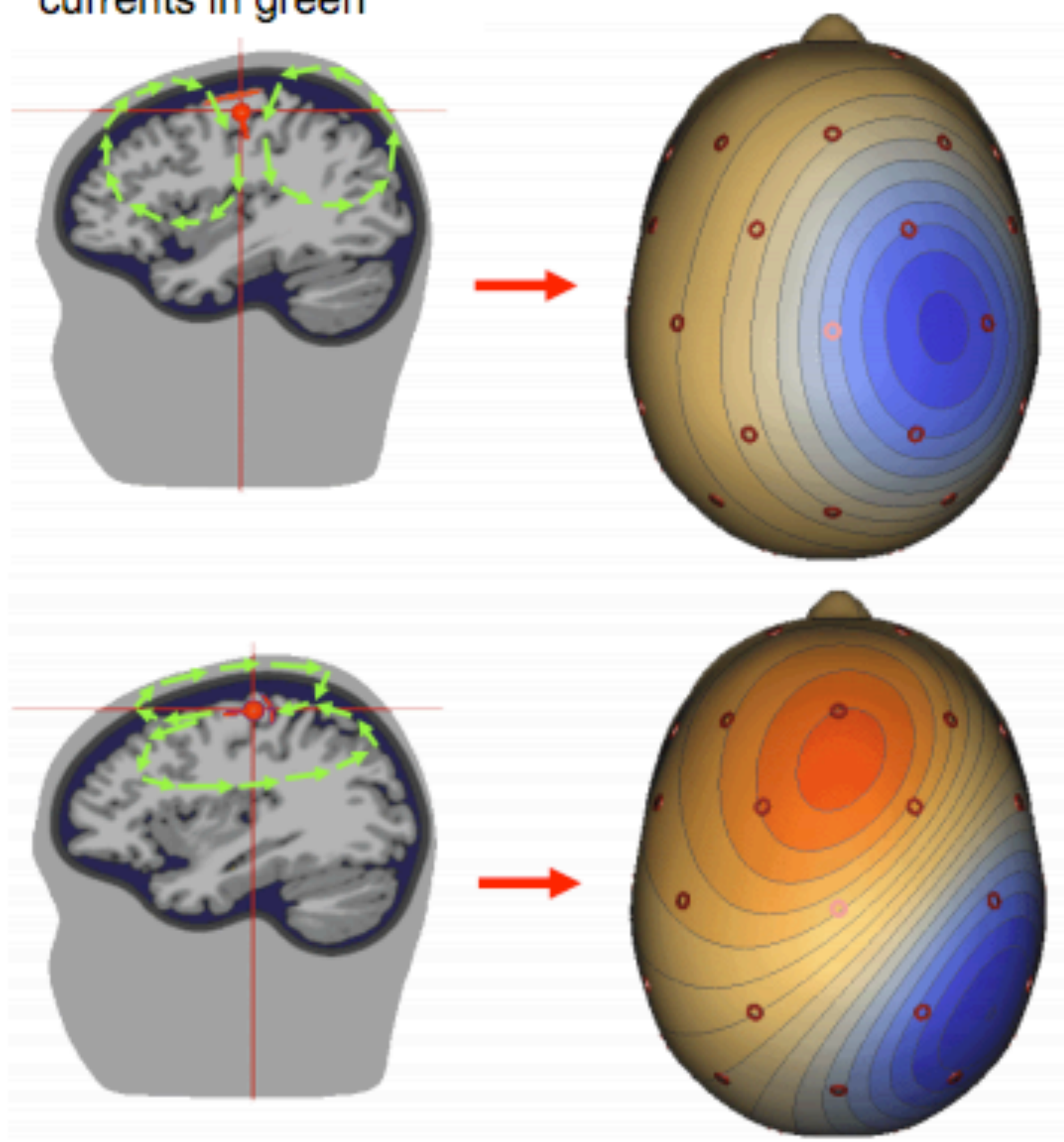

Top: Radial primary current flow at the cortical convexity in the right central cortex.

Bottom: Tangential primary current flow in a cortical fissure.

Although the location of the active brain region is nearly the same, the different orientation of the patch surfaces and the associated different flow of the secondary volume currents lead to a completely different potential distribution. Maximum EEG activity is not necessarily generated directly on top of the active brain region.

B EEG of awake human

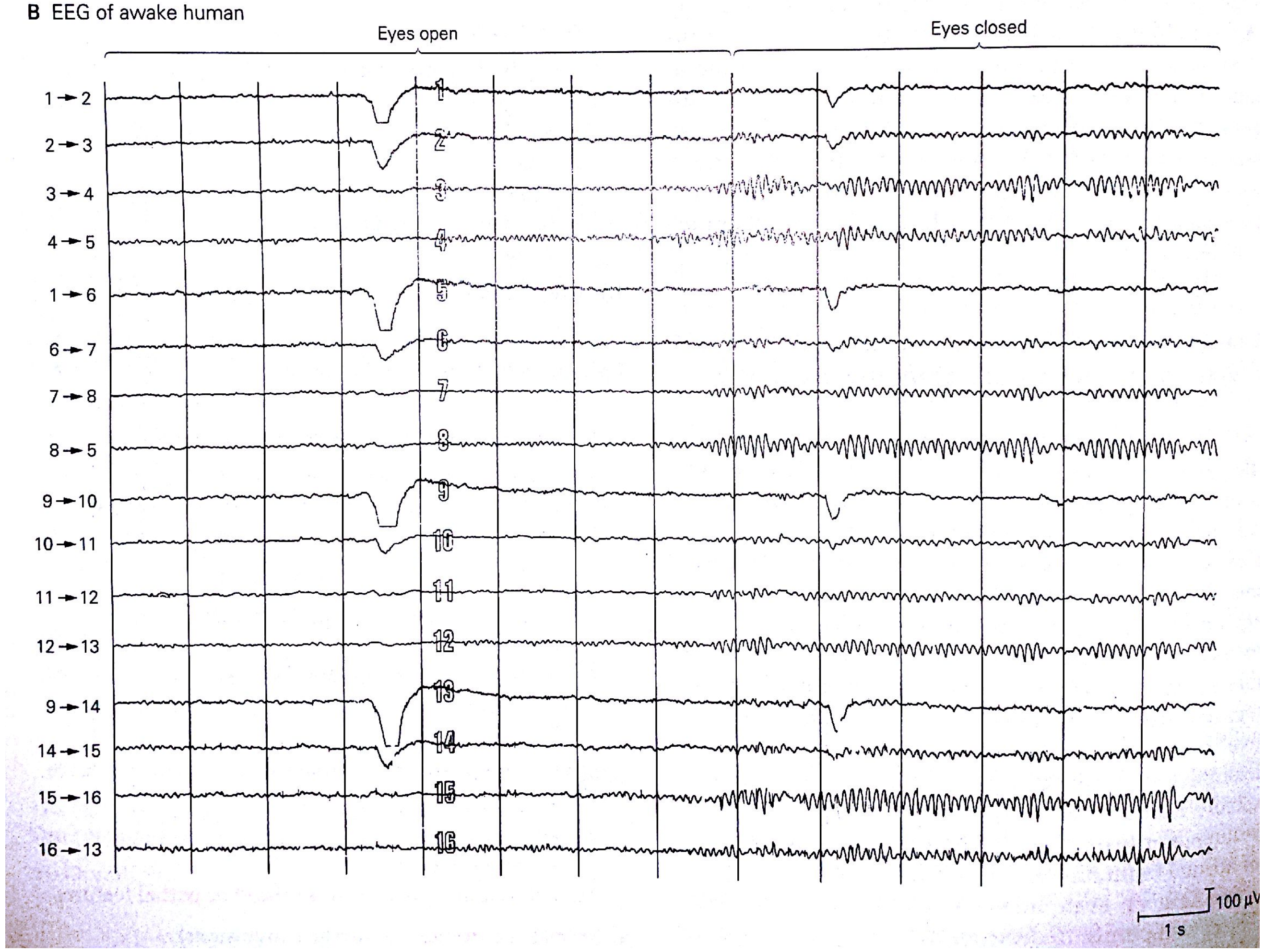

A Spike and wave activity in typical absence seizure

Source localization

Scalp Topography

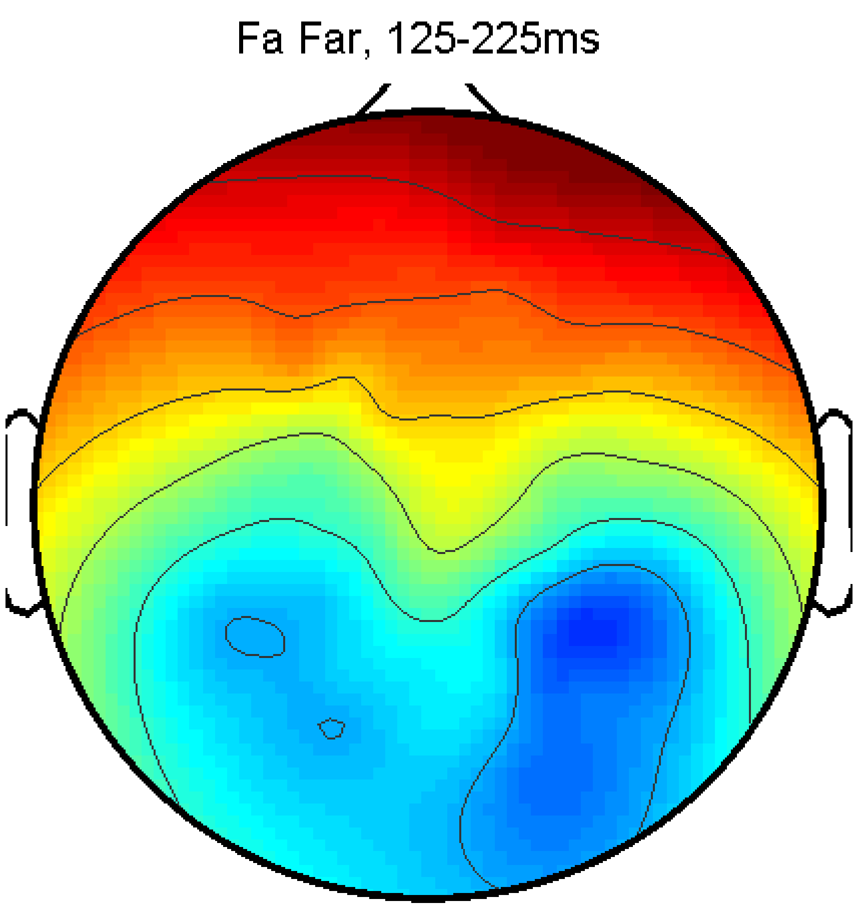

Source localization

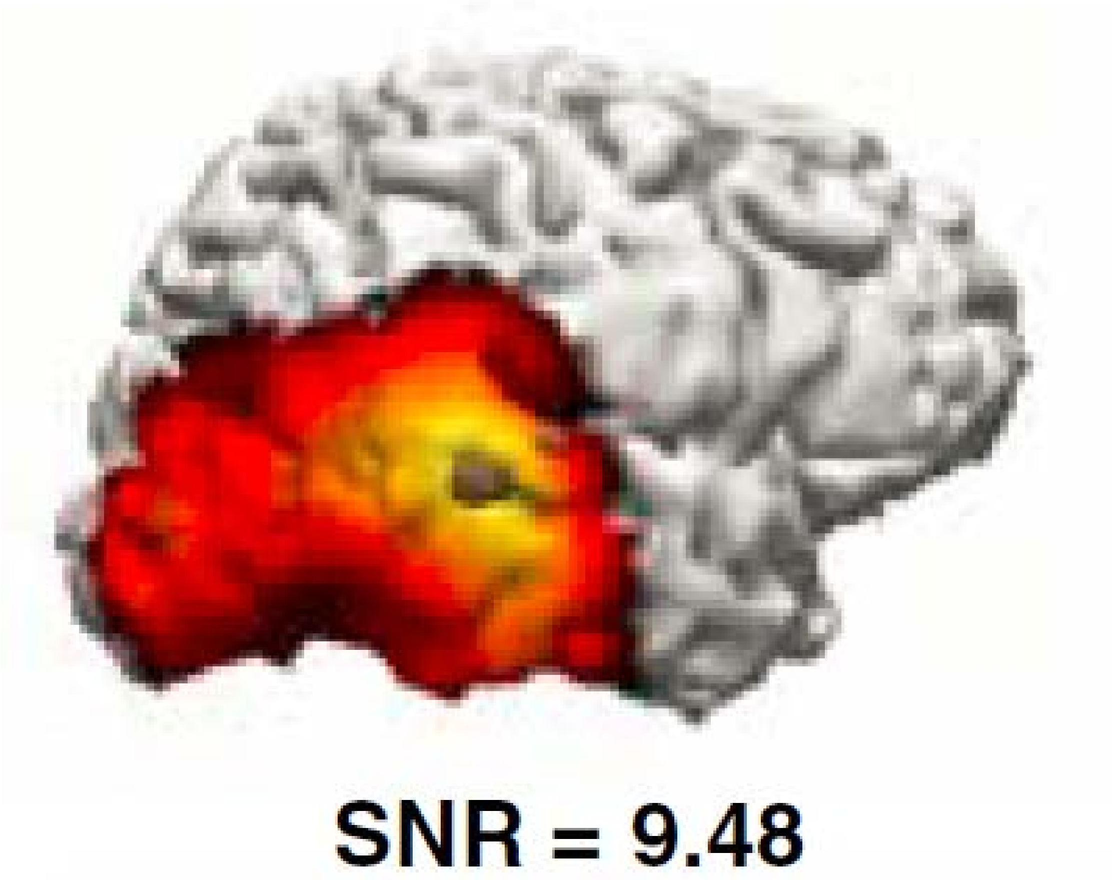

Ponton, C. W., Bernstein, L. E., & Auer, E. T. (2009). Mismatch negativity with visual-only and audiovisual speech. *Brain Topography, 21(3-4), 207-215.*

Constrained localization

$$\mathbf{v} = \mathbf{E}\mathbf{s}$$

$$\mathbf{m} = \mathbf{B}\mathbf{s}$$

$$\mathbf{x} = \mathbf{A}\mathbf{s}, \text{ where } \mathbf{x} = \begin{bmatrix}\mathbf{v}\\ \mathbf{m}\end{bmatrix}, \ \mathbf{A} = \begin{bmatrix}\mathbf{E}\\ \mathbf{B}\end{bmatrix}$$

$$\mathbf{x} = \mathbf{A}\mathbf{s} + \mathbf{n}$$

$$Err_W = \langle \| \mathbf{W}\mathbf{x} - \mathbf{s} \|^2 \rangle$$

$$Err_W = \left\langle \left\| Wx - s \right\|^2 + \lambda \left\| W^{-1} - A \right\|^{\alpha} \right\rangle$$

$$Err_W = \langle \| \mathbf{W}(\mathbf{A}\mathbf{s} + \mathbf{n}) - \mathbf{s} \|^2 \rangle$$

$$= \langle \| (\mathbf{W}\mathbf{A} - \mathbf{I})\mathbf{s} + \mathbf{W}\mathbf{n} \|^2 \rangle$$

$$= \langle \| \mathbf{M}\mathbf{s} + \mathbf{W}\mathbf{n} \|^2 \rangle, \text{ where } \mathbf{M} = \mathbf{W}\mathbf{A} - \mathbf{I}$$

$$= \langle \| \mathbf{M}\mathbf{s} \|^2 \rangle + \langle \| \mathbf{W}\mathbf{n} \|^2 \rangle$$

$$= Tr(\mathbf{M}\mathbf{R}\mathbf{M}^{\mathrm{T}}) + Tr(\mathbf{W}\mathbf{C}\mathbf{W}^{\mathrm{T}})$$

$$\mathbf{W} = \mathbf{R}\mathbf{A}^{\mathrm{T}}(\mathbf{A}\mathbf{R}\mathbf{A}^{\mathrm{T}} + \mathbf{C})^{-1}$$

Dale & Sereno (1993)

Event-related potential

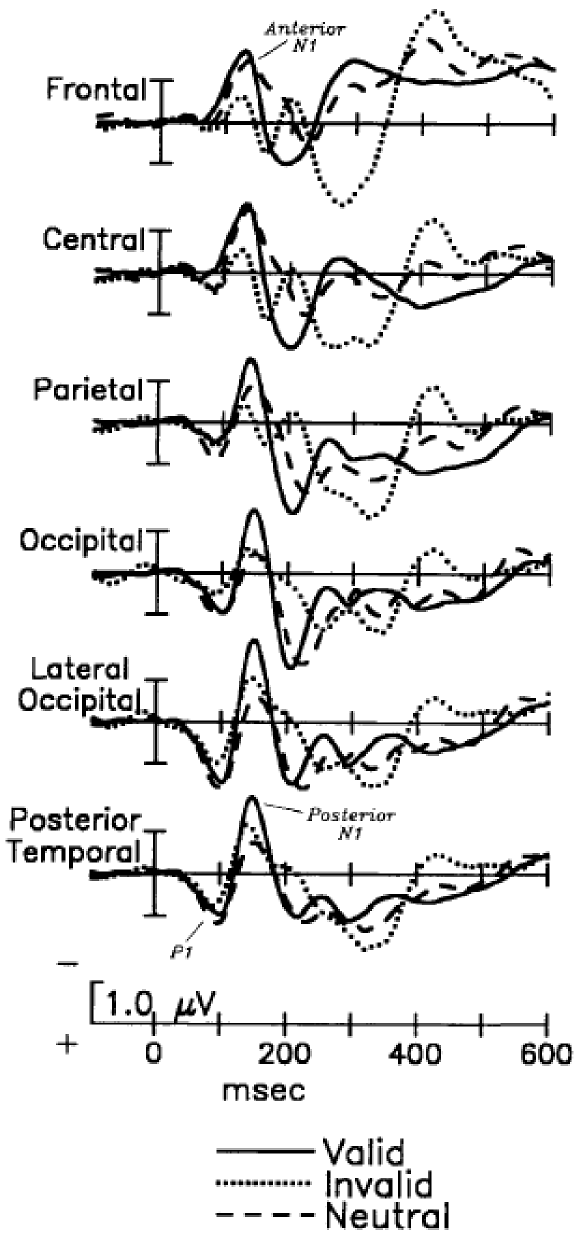

- erpology: the study of how experimental manipulations change ERP component latency/amplitude
  - Making the connection b/w an ERP effect and a brain effect can be tricky
- Recommended reading:
  - Luck, S. (2005). *An Introduction to the Event-Related Potential Technique: The MIT Press, Cambridge MA.*
- Some "Gotchas" while reading ERP papers:
  - Not everyone uses the same reference electrode
  - Sometimes negative is up
  - Beware of spatial claims
  - Cherry-picking is standard practice
  - Beware of biased measures

The good, the bad ...

- Cheap, easy to use
- High temporal resolution
- Clinical use for anesthesia, epilepsy
- Research use for sleep, attention, cognition, perception
- Very poor spatial resolution
- Many artifacts: eye movement, blinking, facial gestures, heart activity

Frequency Spectrum

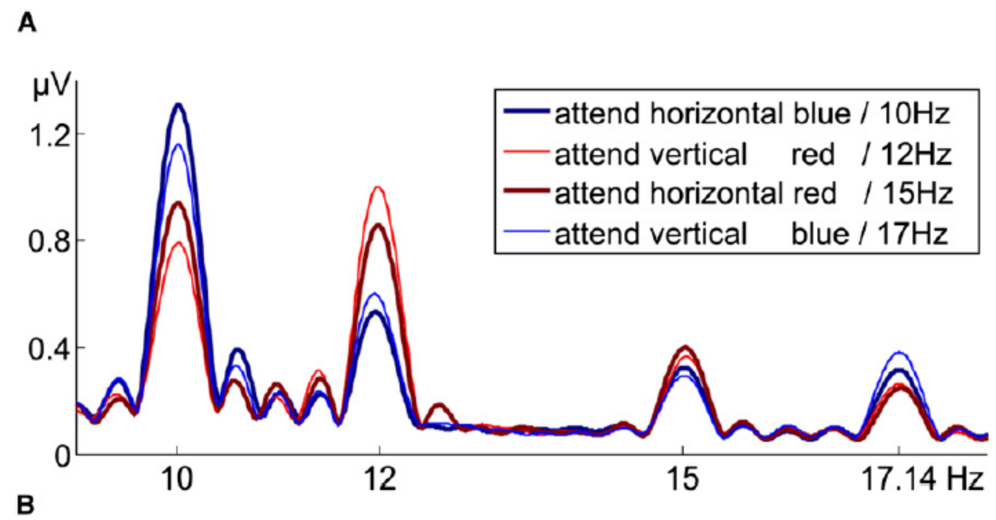

Andersen, S. K., Hillyard, S. A., & Müller, M. M. (2008). Attention facilitates multiple stimulus features in parallel in human visual cortex. *Current Biology, 18(13), 1006-1009.*

- SSVEP
- Traditional frequency bands:
  - Delta (1-4 Hz)
  - Theta (4-8 Hz)
  - Alpha (8-12 Hz)
  - Beta (12-24 Hz)
  - Gamma (30 & up)

Time/Frequency

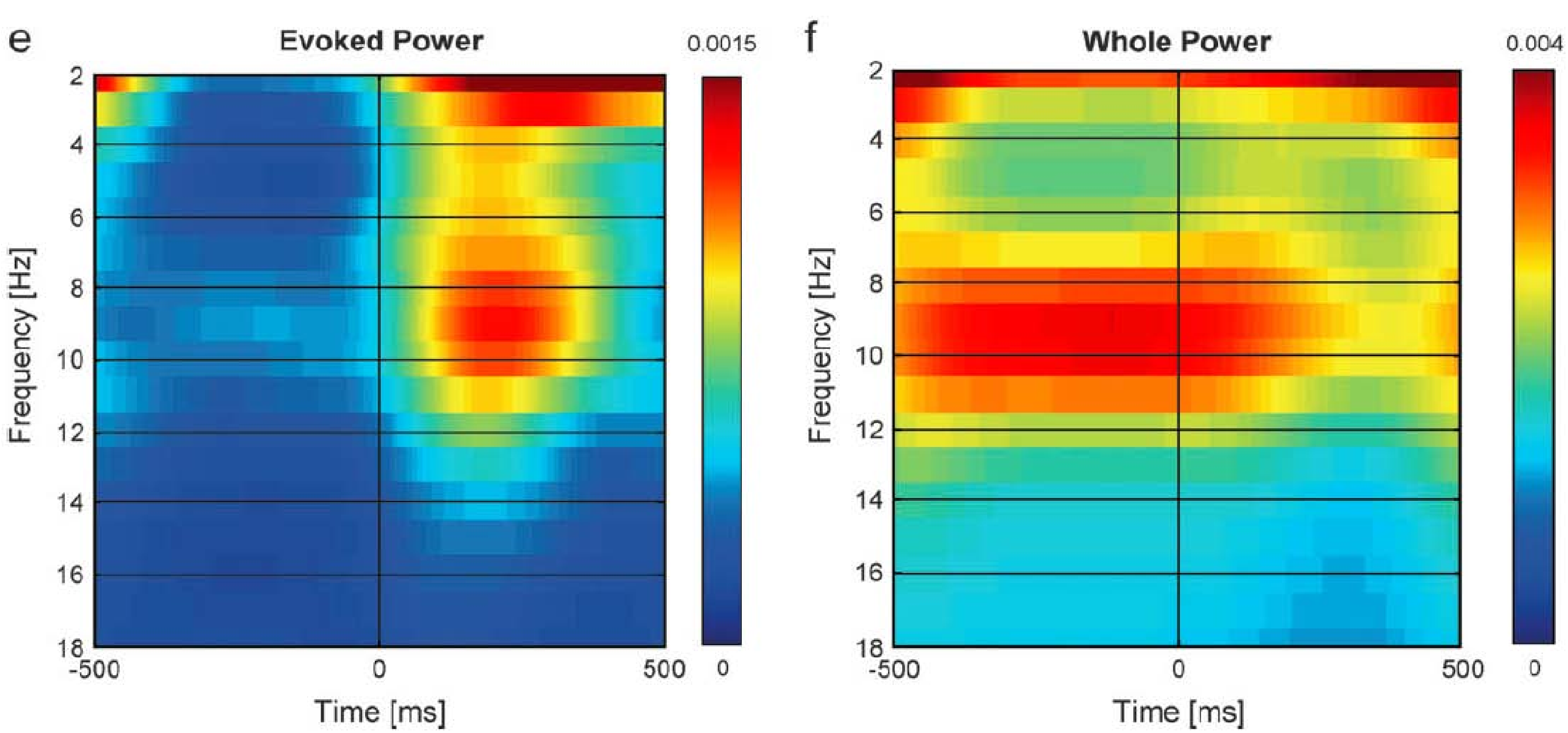

What’s it good for

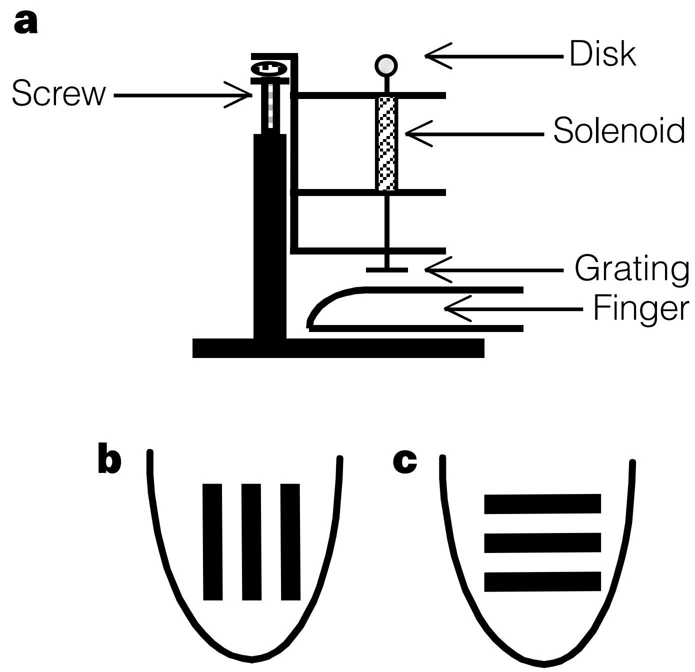

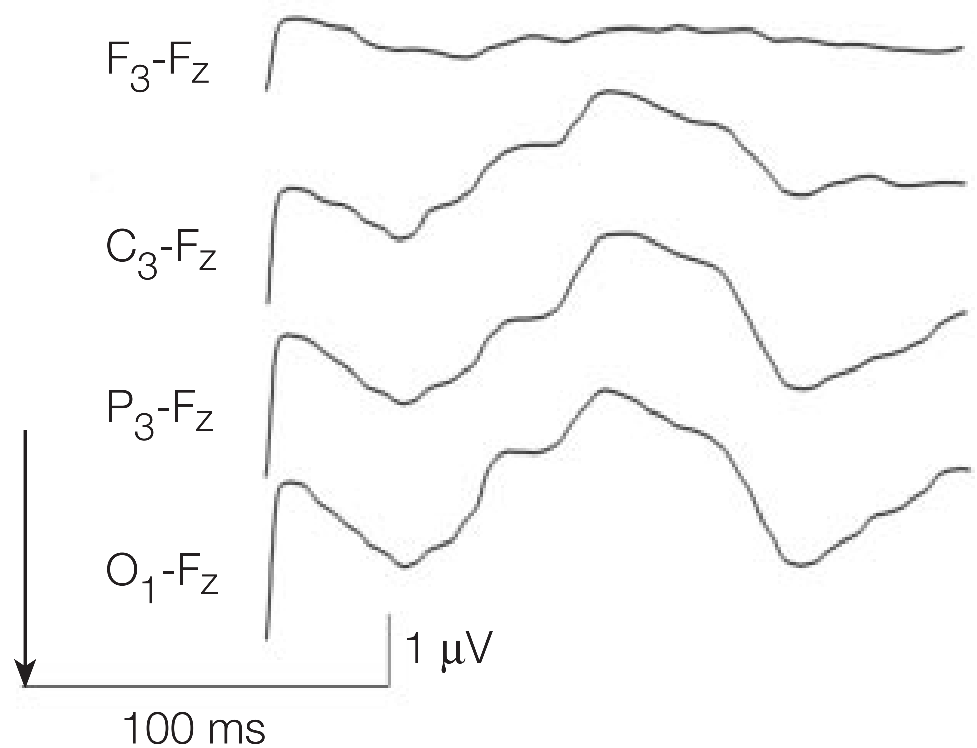

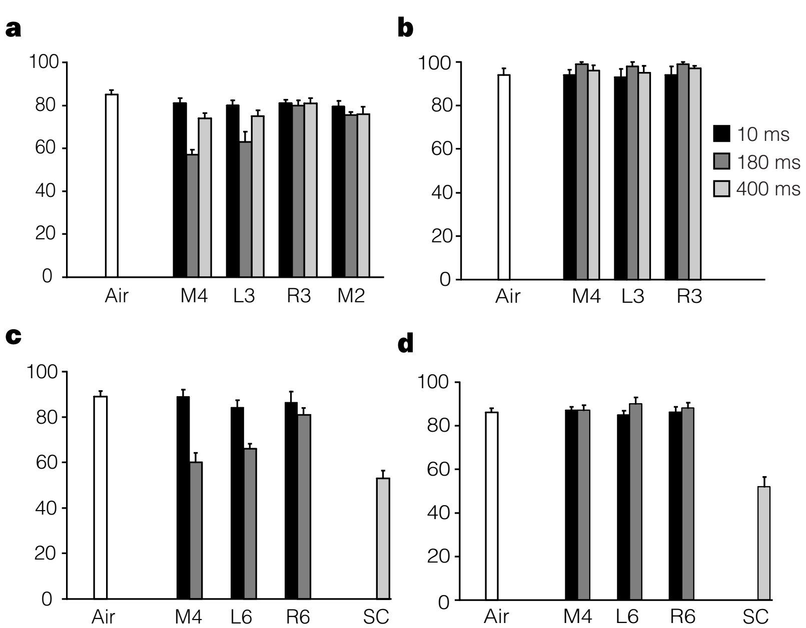

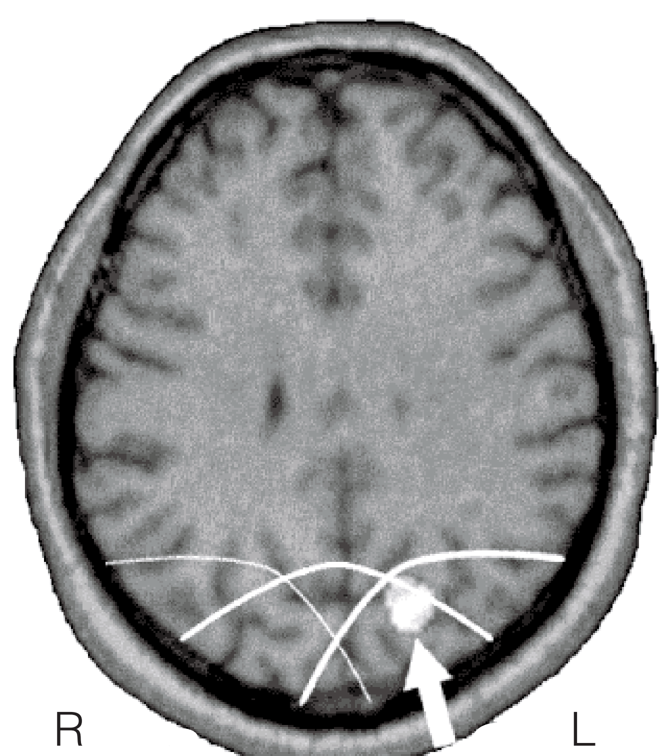

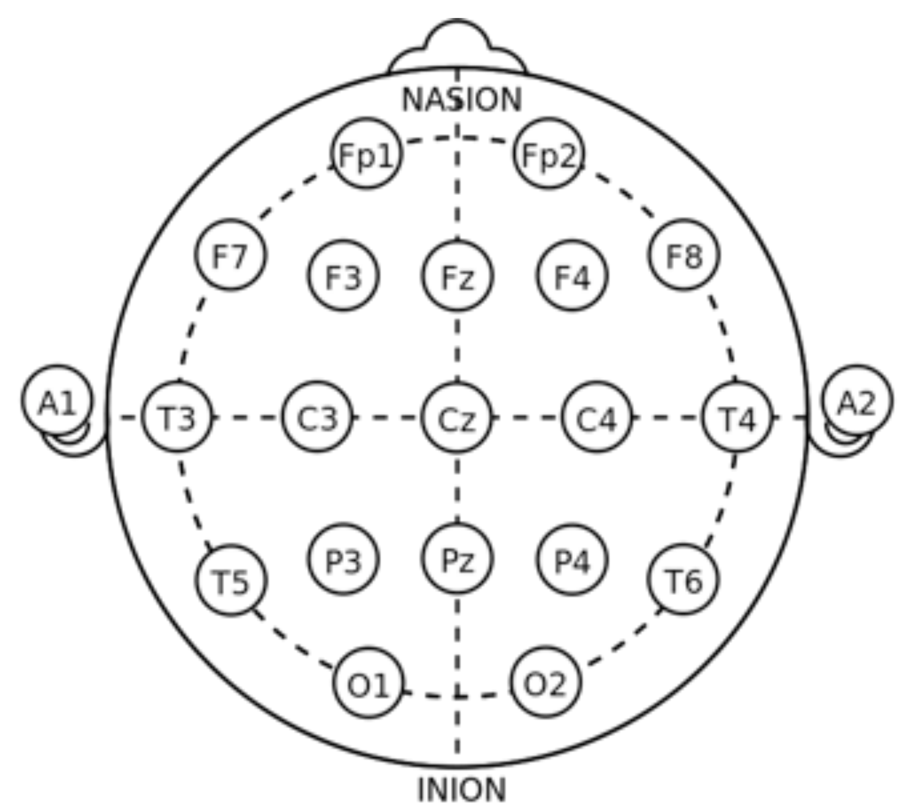

Zangaladze (1999)

What's it good for

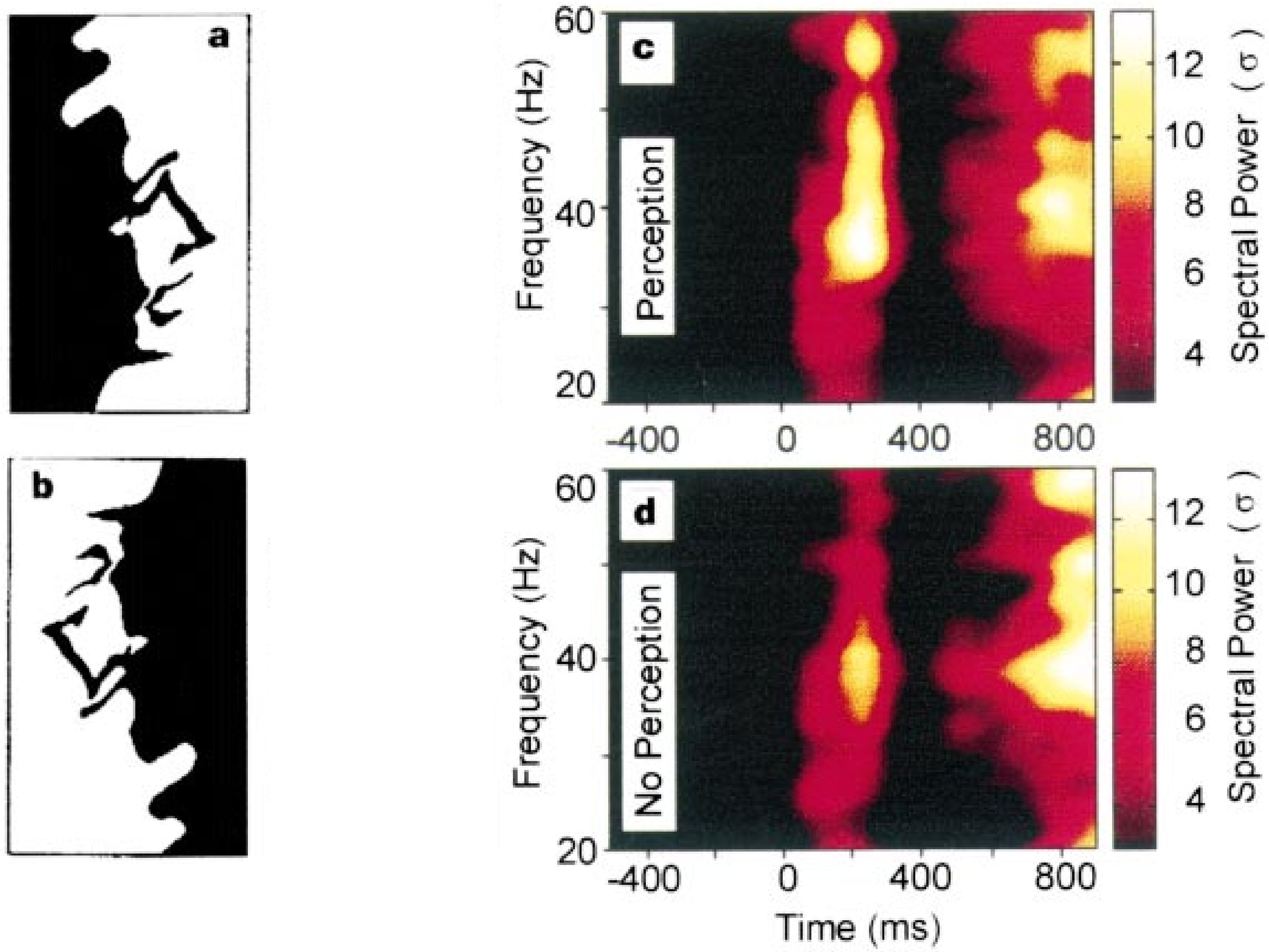

Varela (1999)

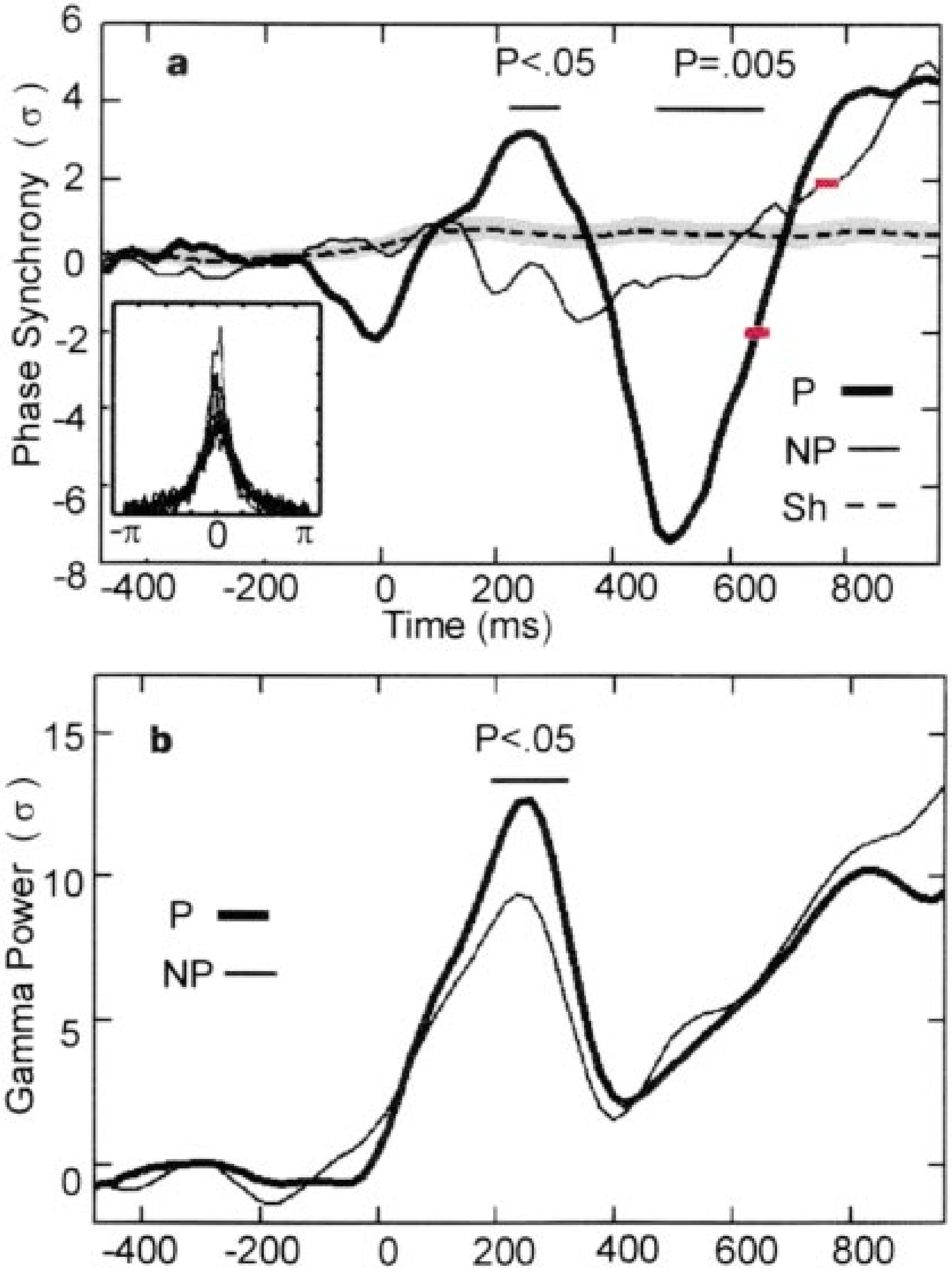

a
P<.05
P=.005
Phase Synchrony (σ)
6
4
2
0
-2
-4
-6
-8
-π
0
π
P
NP
Sh
-400
-200
0
200
400
600
800
Time (ms)
b
P<.05
Gamma Power (σ)
15
10
5
0
P
NP
-400
-200
0
200
400
600
800

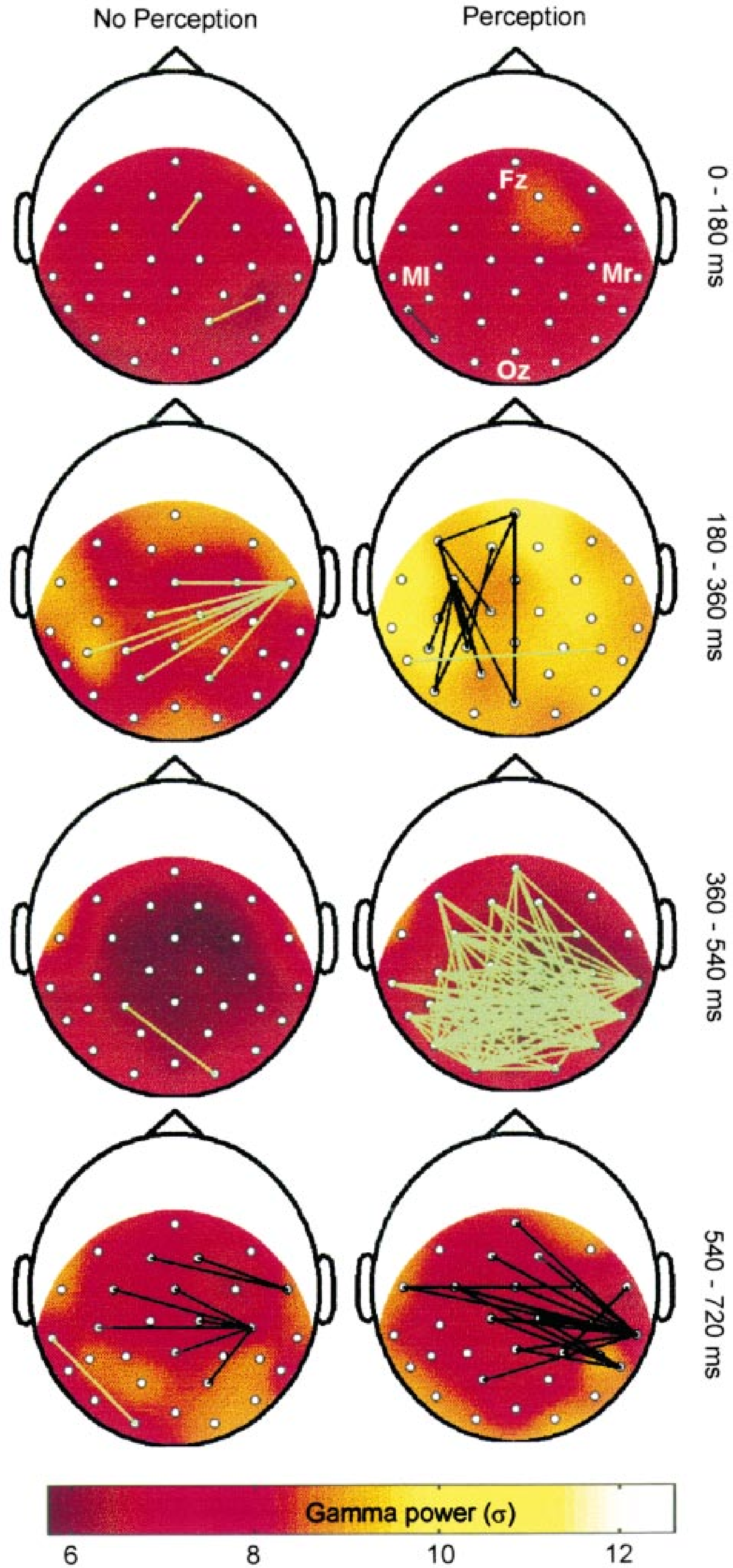

No Perception
Perception
0 - 180 ms
180 - 360 ms
360 - 540 ms
540 - 720 ms
Fz
Ml
Mr
Oz
Gamma power (σ)
6
8
10
12

Correlation is not causation, right?

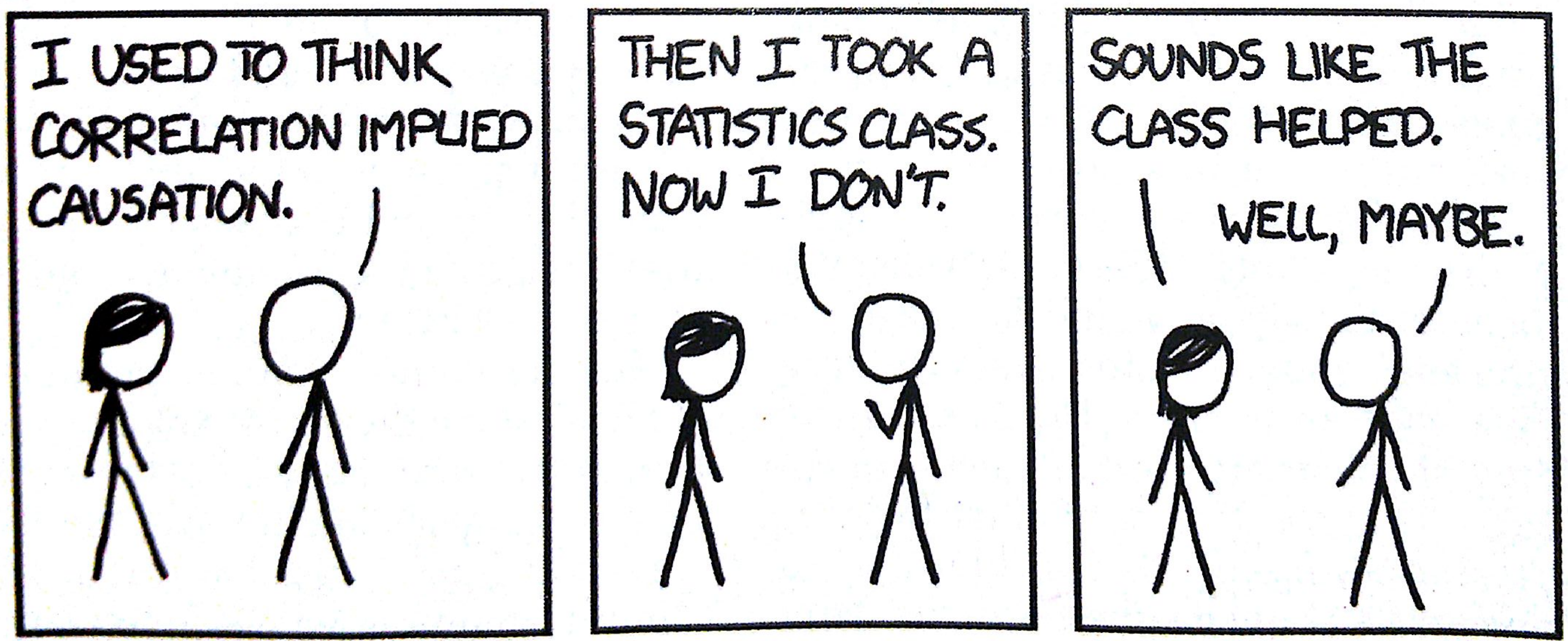

Big data

- Cheap sets
  - ✓ Neurosky, eMotiv
  - ✓ Toys, games (Mindflex)
  - ✓ Kickstarter project
  - ✓ Carnegie Mellon (Bryan Murphy)
- Massive repositories
  - ✓ G. Church - Harvard

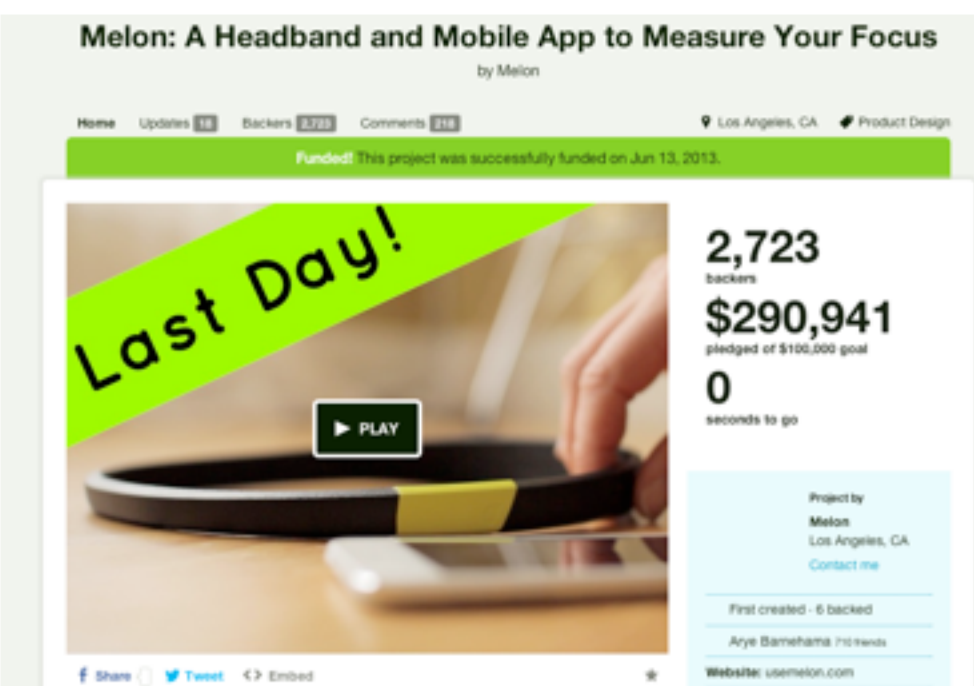

... and the ugly

Electrocorticography (ECoG)

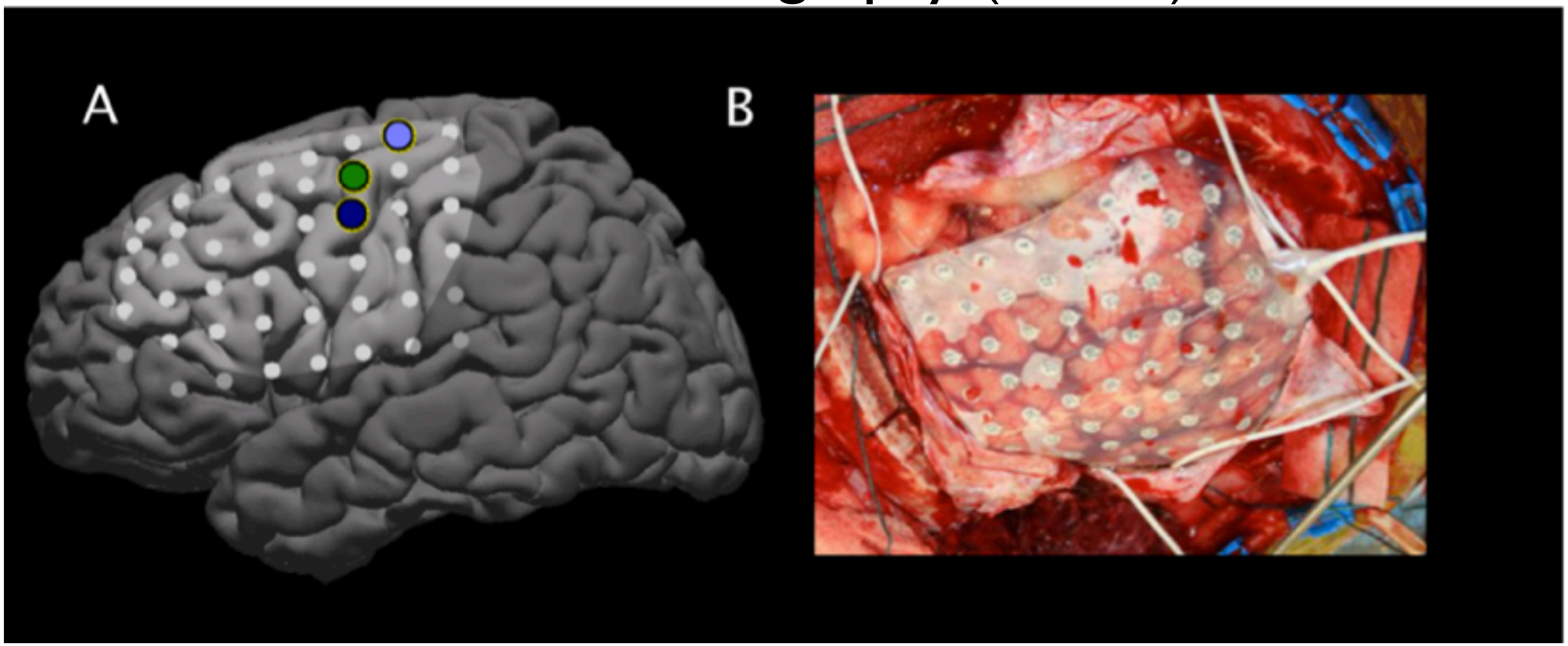

- Electrodes under the dura
- Many fewer artifacts (eyes, facial, scalp diffusion)
- Limited used in humans: epileptic ablation pre-operative guidance

Flexible, foldable, actively multiplexed, high-density electrode array for mapping brain activity *in vivo*

- *Nature Neuroscience*, Dec. 2011

Jonathan Viventi[1,2,13], Dae-Hyeong Kim[3,13], Leif Vigeland[4], Eric S Frechette[5], Justin A Blanco[6], Yun-Soung Kim[7], Andrew E Avrin[8], Vineet R Tiruvadi[9], Suk-Won Hwang[7], Ann C Vanleer[9], Drausin F Wulsin[9], Kathryn Davis[5], Casey E Gelber[9], Larry Palmer[4], Jan Van der Spiegel[8], Jian Wu[10], Jianliang Xiao[11], Yonggang Huang[12], Diego Contreras[4], John A Rogers[7] & Brian Litt[5,9]

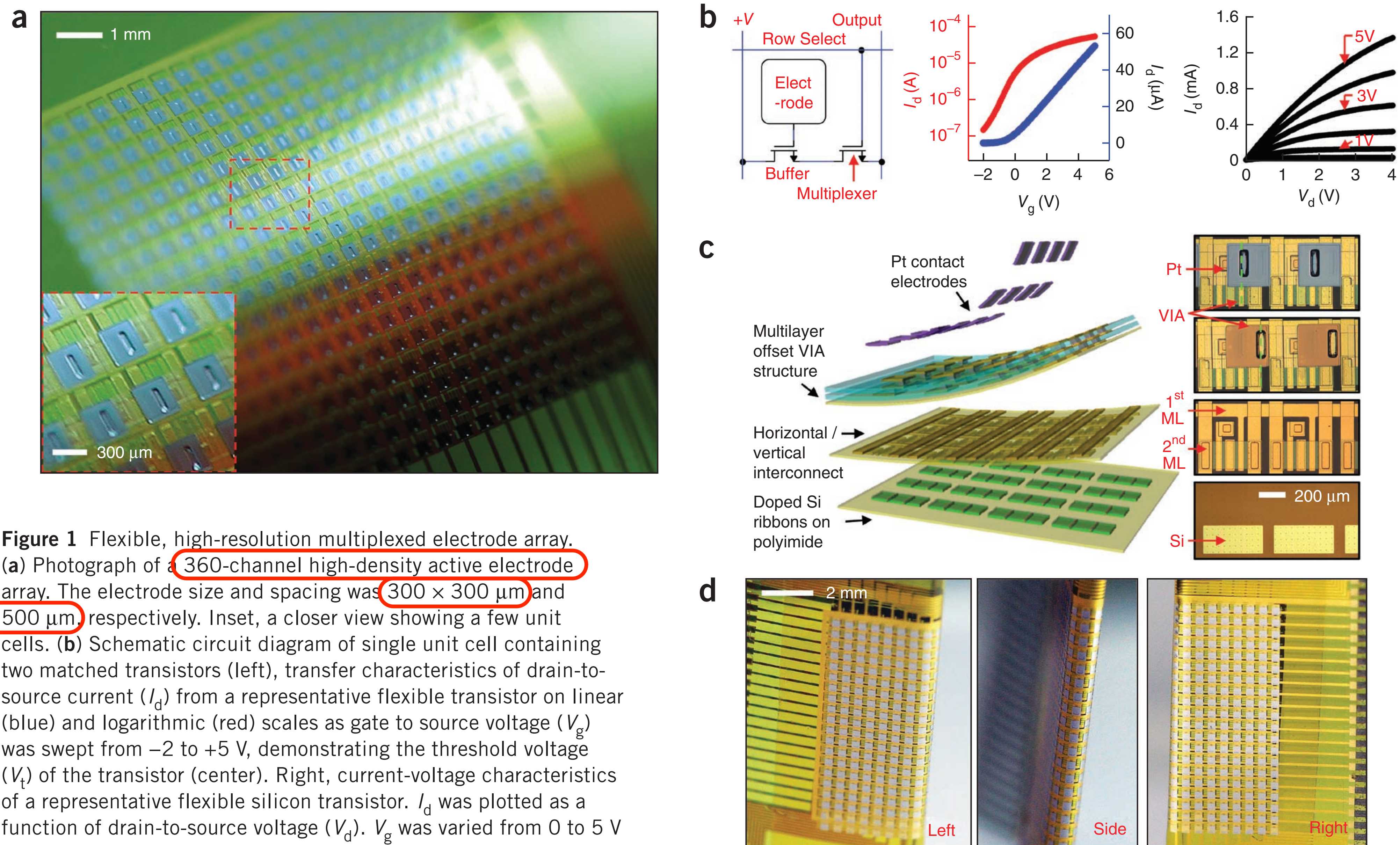

Figure 1 Flexible, high-resolution multiplexed electrode array. (**a**) Photograph of a 360-channel high-density active electrode array. The electrode size and spacing was 300 × 300 μm and 500 μm, respectively. Inset, a closer view showing a few unit cells. (**b**) Schematic circuit diagram of single unit cell containing two matched transistors (left), transfer characteristics of drain-to-source current (I_d) from a representative flexible transistor on linear (blue) and logarithmic (red) scales as gate to source voltage (V_g) was swept from −2 to +5 V, demonstrating the threshold voltage (V_t) of the transistor (center). Right, current-voltage characteristics of a representative flexible silicon transistor. I_d was plotted as a function of drain-to-source voltage (V_d). V_g was varied from 0 to 5 V in 1-V steps. (**c**) Schematic exploded view (left) and corresponding microscope image of each layer: doped silicon nanoribbons (right frame, bottom), after vertical and horizontal interconnection with arrows indicating the first and second metal layers (ML, right frame, second from bottom), after water-proof encapsulation (right frame, third from bottom) and after platinum electrode deposition (right frame, top). Green dashed lines illustrated the offset via structure, critical for preventing leakage current while submerged in conductive fluid. (**d**) Images of folded electrode array around low modulus polydimethylsiloxane (PDMS) insert. (**e**) Bending stiffness of electrode array for varying epoxy thicknesses and two different polyimide (PI) substrate thicknesses. A nearly tenfold increase in flexibility between the current device and our prior work was shown. (**f**) Induced strain in different layers depending on the change in bending radius.

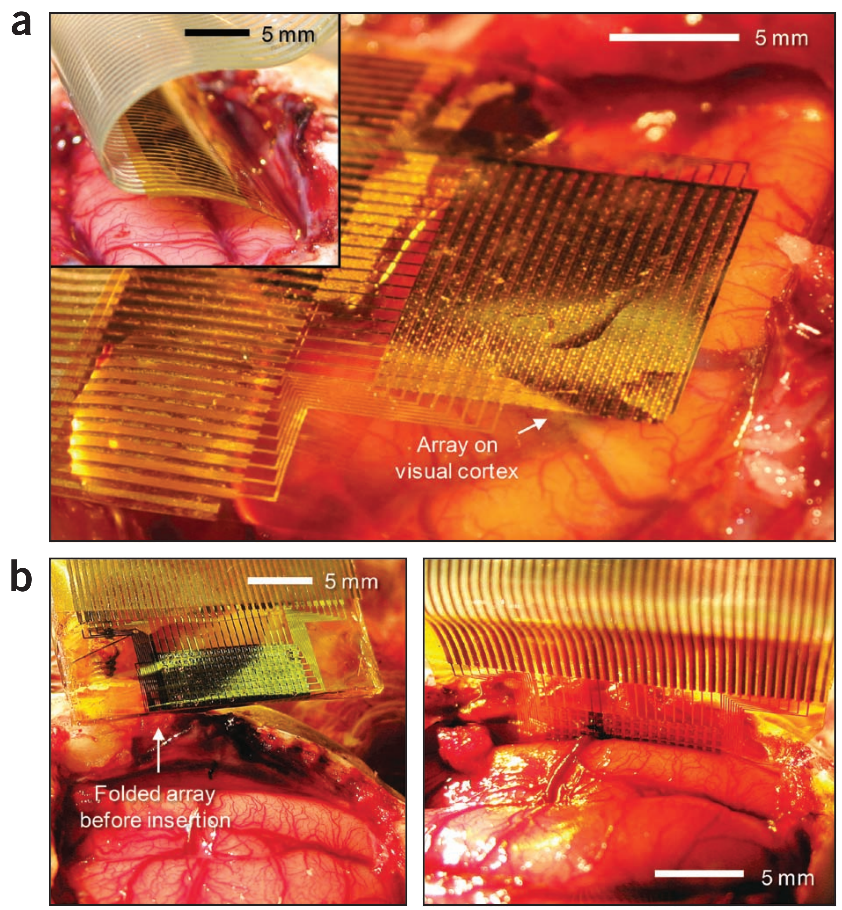

- Multiplexing along column, speed <5µsec
- Sampling rate > 10kS/sec
- Low cross-talk
- Sampling area 10 x 9 mm
- Claim: sample 80 x 80 mm, 25,600 channels at > 1.2 kS/sec

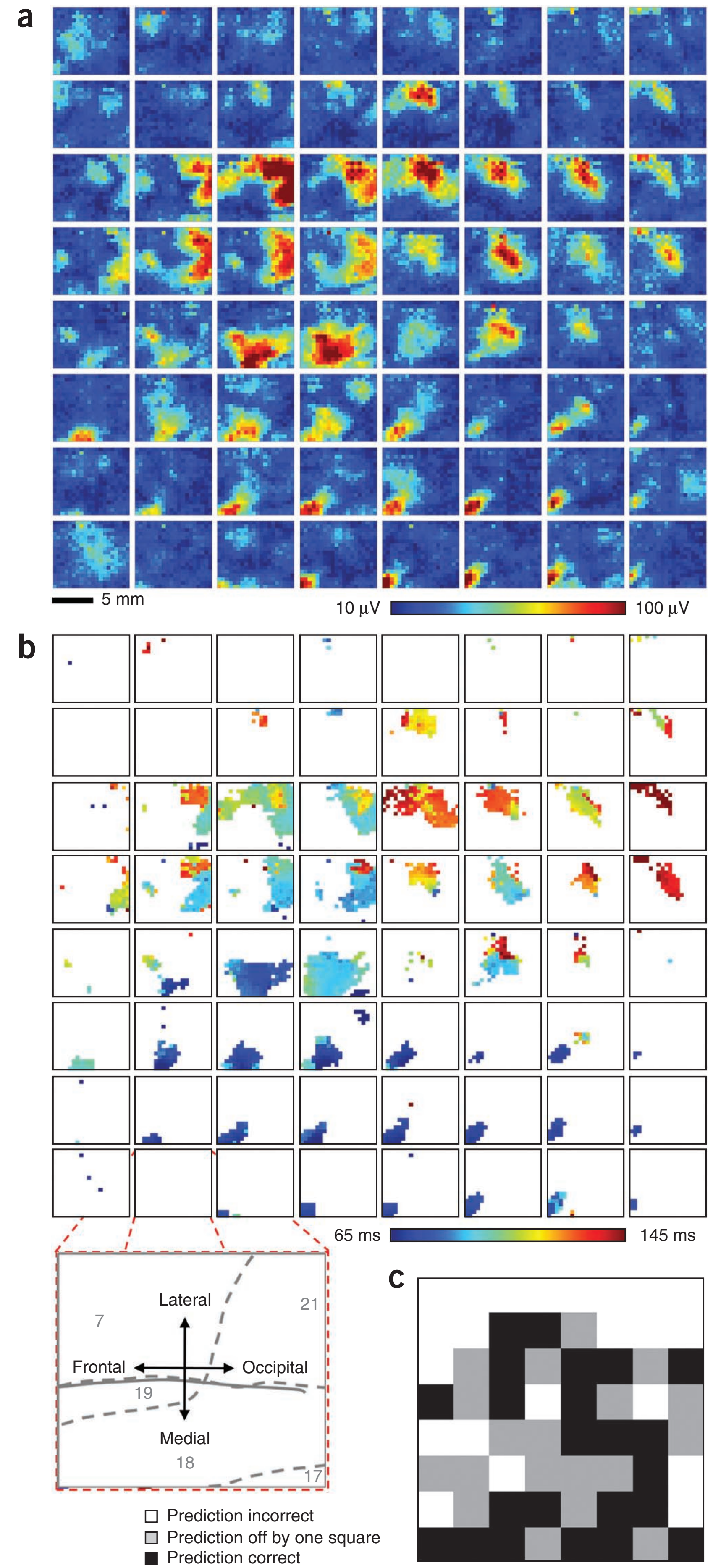

Finger Movement Classification for an Electrocorticographic BCI

Pradeep Shenoy Kai J. Miller Jeffrey G. Ojemann Rajesh P.N. Rao
Dept. of Computer Science and Engineering
University of Washington
{pshenoy,kai,rao}@cs.washington.edu, jeff.ojemann@seattlechildrens.org

- *Neural Engineering*, 2007

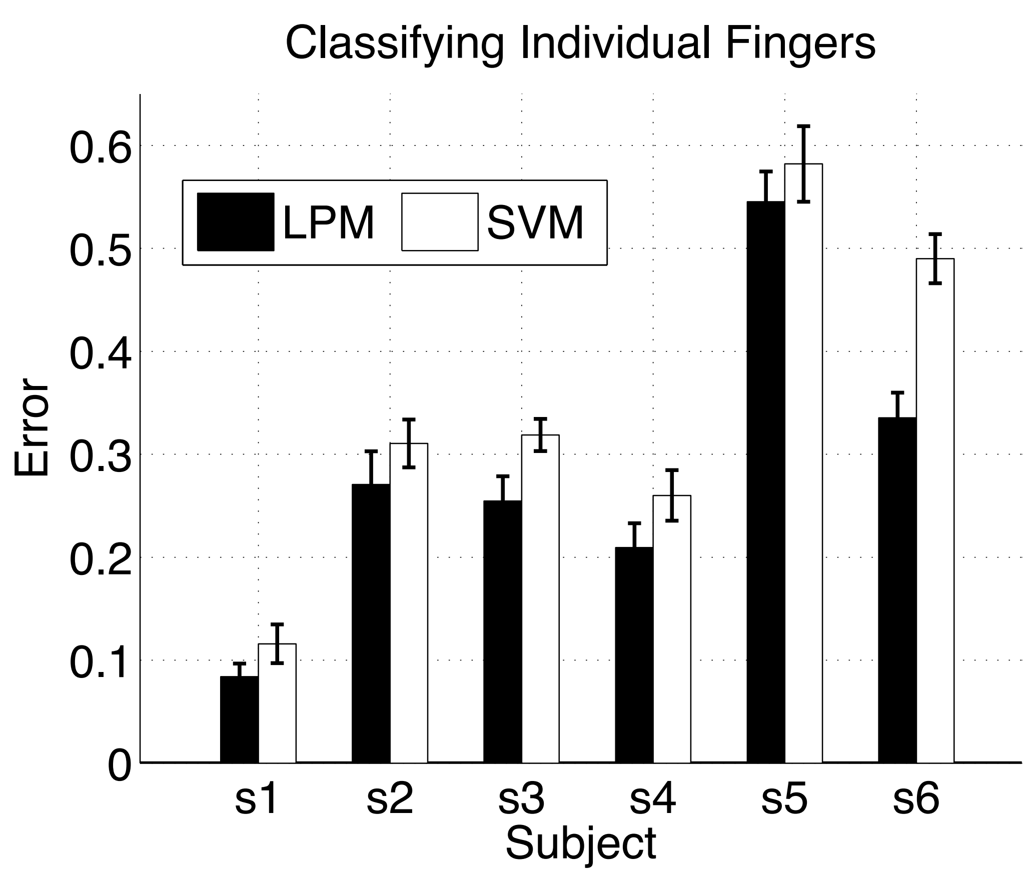

Fig. 1. **Classifying finger movement activity:** The figure shows the 5-class cross-validation error for the LPM and SVM classifiers, across 6 subjects. The results show that a high degree of accuracy is possible in distinguishing individual finger movements using ECOG. Also, the LPM consistently outperforms the SVM. (Chance level for a 5-class problem is 80% error.)

Reconstructing Speech from Human Auditory Cortex

Brian N. Pasley[1]*, Stephen V. David[2], Nima Mesgarani[2,3], Adeen Flinker[1], Shihab A. Shamma[2], Nathan E. Crone[4], Robert T. Knight[1,3,5], Edward F. Chang[3]

1 Helen Wills Neuroscience Institute, University of California Berkeley, Berkeley, California, United States of America, **2** Institute for Systems Research and Department of Electrical and Computer Engineering, University of Maryland, College Park, Maryland, United States of America, **3** Department of Neurological Surgery, University of California–San Francisco, San Francisco, California, United States of America, **4** Department of Neurology, The Johns Hopkins University, Baltimore, Maryland, United States of America, **5** Department of Psychology, University of California Berkeley, Berkeley, California, United States of America

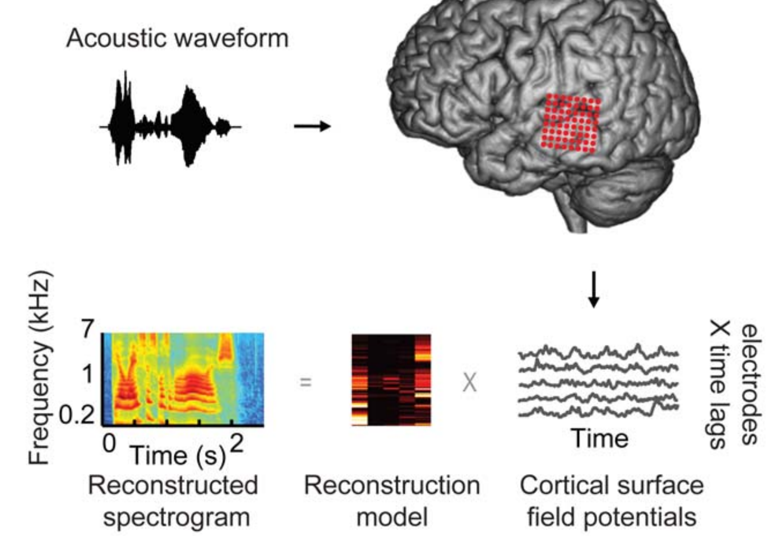

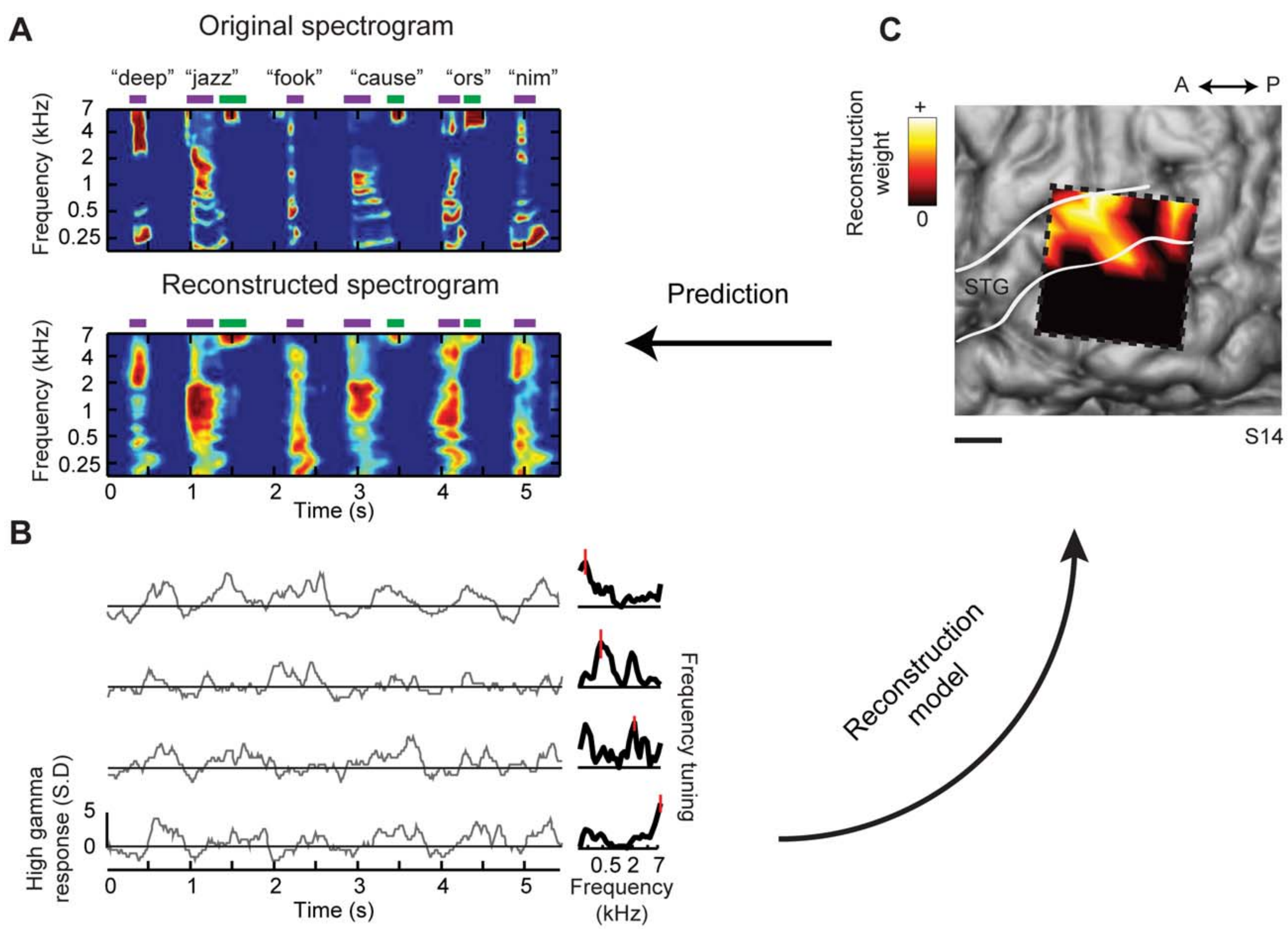

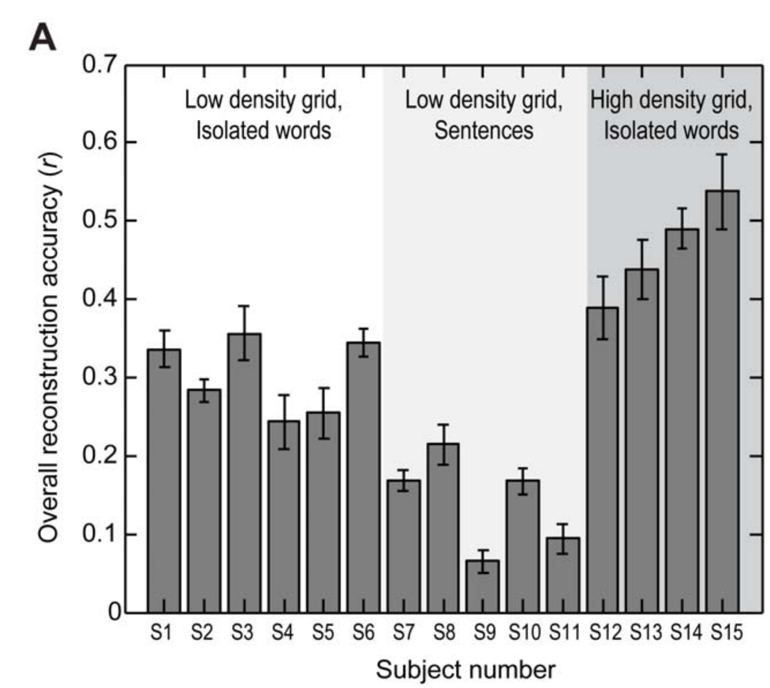

Improved reconstruction adding wavelet analysis, to account for frequency sweeps

Epidermal Electronics

Dae-Hyeong Kim,[1]* Nanshu Lu,[1]* Rui Ma,[2]* Yun-Soung Kim,[1] Rak-Hwan Kim,[1] Shuodao Wang,[3] Jian Wu,[3] Sang Min Won,[1] Hu Tao,[4] Ahmad Islam,[1] Ki Jun Yu,[1] Tae-il Kim,[1] Raeed Chowdhury,[2] Ming Ying,[1] Lizhi Xu,[1] Ming Li,[3,6] Hyun-Joong Chung,[1] Hohyun Keum,[1] Martin McCormick,[2] Ping Liu,[5] Yong-Wei Zhang,[5] Fiorenzo G. Omenetto,[4] Yonggang Huang,[3] Todd Coleman,[2] John A. Rogers[1]†

We report classes of electronic systems that achieve thicknesses, effective elastic moduli, bending stiffnesses, and areal mass densities matched to the epidermis. Unlike traditional wafer-based technologies, laminating such devices onto the skin leads to conformal contact and adequate adhesion based on van der Waals interactions alone, in a manner that is mechanically invisible to the user. We describe systems incorporating electrophysiological, temperature, and strain sensors, as well as transistors, light-emitting diodes, photodetectors, radio frequency inductors, capacitors, oscillators, and rectifying diodes. Solar cells and wireless coils provide options for power supply. We used this type of technology to measure electrical activity produced by the heart, brain, and skeletal muscles and show that the resulting data contain sufficient information for an unusual type of computer game controller.

12 AUGUST 2011 VOL 333 **SCIENCE**

Startup out of Physics Dept., Univ. of Illinois Urbana-Champaigne

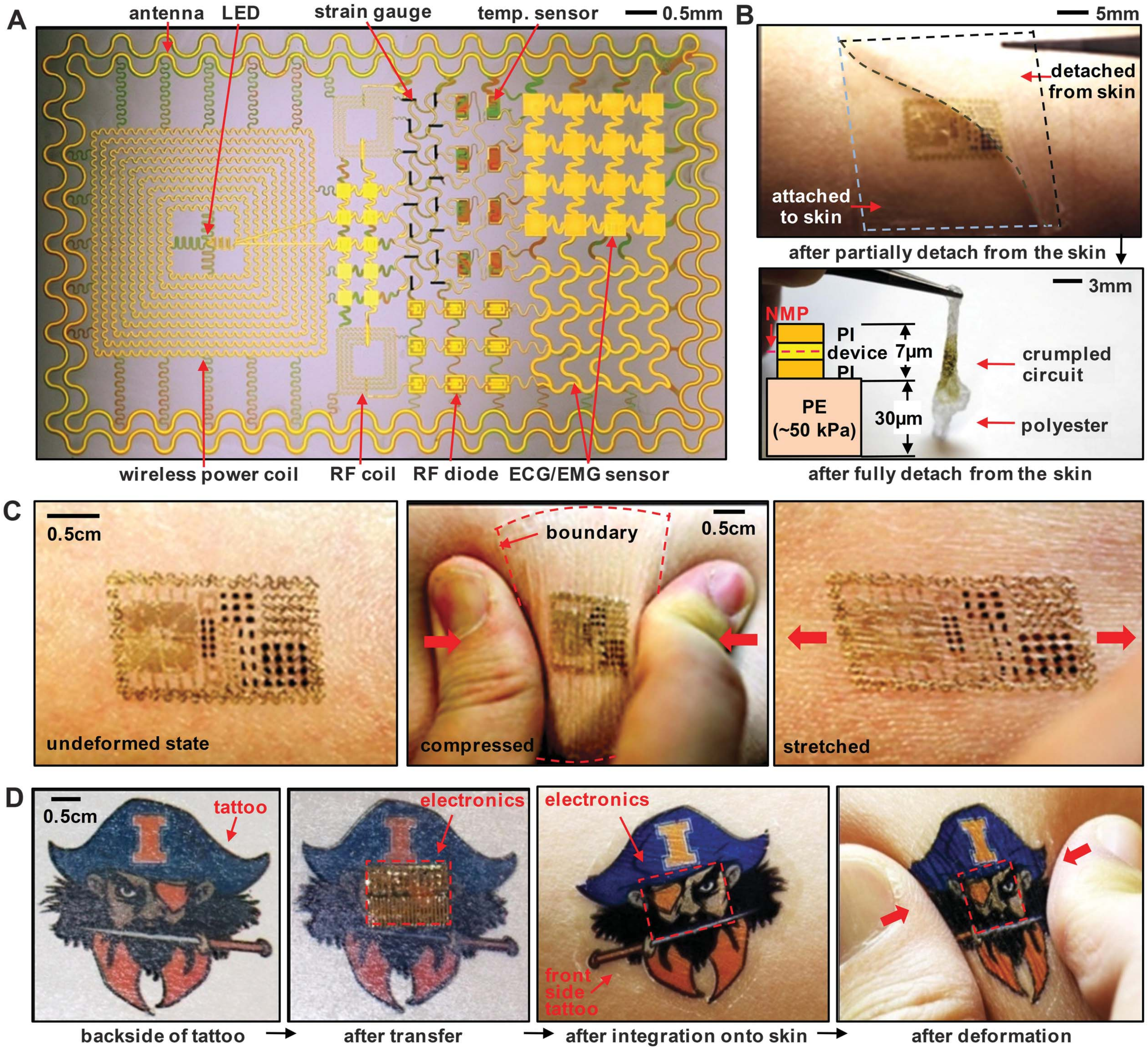

A demonstrative platform is shown in Fig. 1, integrating a collection of multifunctional sensors (such as temperature, strain, and electrophysiological), microscale light-emitting diodes (LEDs), active/passive circuit elements (such as transistors, diodes, and resistors), wireless power coils, and devices for radio frequency (RF) communications (such as high-frequency inductors, capacitors, oscillators, and antennae), all integrated on the surface of a thin (~30 μm), gas-permeable elastomeric sheet based on a modified polyester (BASF, Ludwigshafen, Germany) with low Young's modulus (~60 kPa) (fig. S1A). The devices and interconnects exploit ultrathin layouts (<7 μm), neutral mechanical plane configurations, and optimized geometrical designs. The active elements use established electronic materials, such as silicon and gallium arsenide, in the form of filamentary serpentine nanoribbons and micro- and nanomembranes. The result is a high-performance system that offers reversible, elastic responses to large strain deformations with effective moduli (<150 kPa), bending stiffnesses (<1 nN m), and areal mass densities (<3.8 mg/cm^2) that are orders of magnitude smaller than those possible with conventional electronics or even with recently explored flexible/stretchable device technologies (*10–19*). Water-soluble polymer sheets [polyvinyl alcohol (PVA) (Aicello, Toyohashi, Japan); Young's modulus, ~1.9 GPa; thickness, ~50 μm (fig. S1B)] serve as temporary supports for manual mounting of these systems on the skin in an overall construct that is directly analogous to that of a temporary transfer tattoo. The image in Fig. 1B, top, is of a device similar to the one in Fig. 1A, after mounting it onto the skin by washing away the PVA and then partially

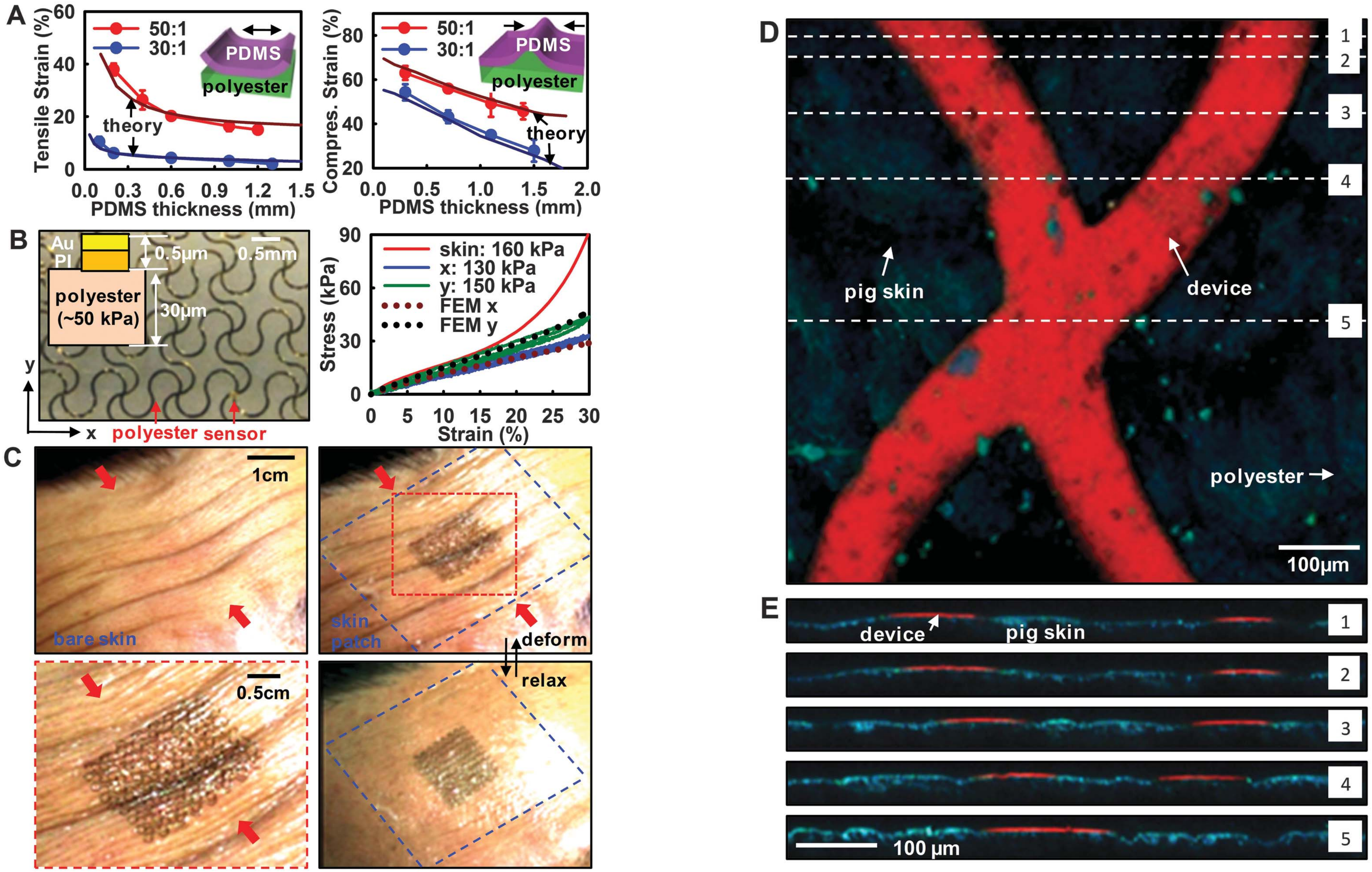

A
Tensile Strain (%)
50:1
30:1
PDMS
polyester
theory
PDMS thickness (mm)
Compres. Strain (%)
50:1
30:1
PDMS
polyester
theory
PDMS thickness (mm)
B
Au
PI
0.5μm
0.5mm
polyester
(~50 kPa)
30μm
y
x
polyester sensor
Stress (kPa)
skin: 160 kPa
x: 130 kPa
y: 150 kPa
FEM x
FEM y
Strain (%)
C
1cm
bare skin
skin patch
deform
relax
0.5cm
D
pig skin
device
polyester
100μm
E
device
pig skin
100 μm

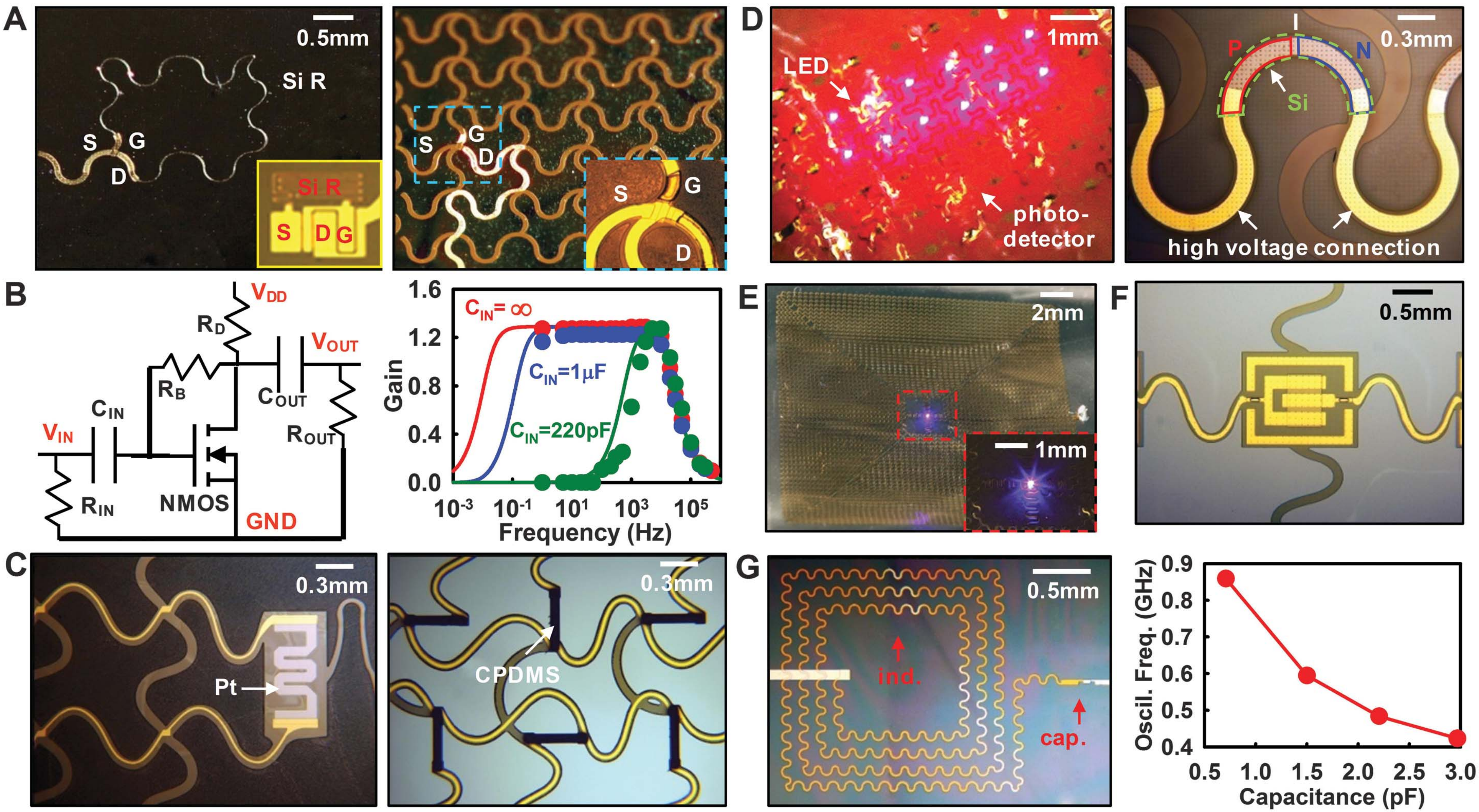

A
0.5mm
Si R
S
G
D
B
V_{DD}
R_D
R_B
V_{OUT}
C_{OUT}
R_{OUT}
C_{IN}
V_{IN}
R_{IN}
NMOS
GND
$C_{IN}=\infty$
$C_{IN}=1\mu F$
$C_{IN}=220pF$
Gain
Frequency (Hz)
C
0.3mm
Pt
CPDMS
D
1mm
LED
photo-detector
P
I
N
Si
high voltage connection
E
2mm
F
G
ind.
cap.
Oscil. Freq. (GHz)
Capacitance (pF)

Electrophysiological recordings

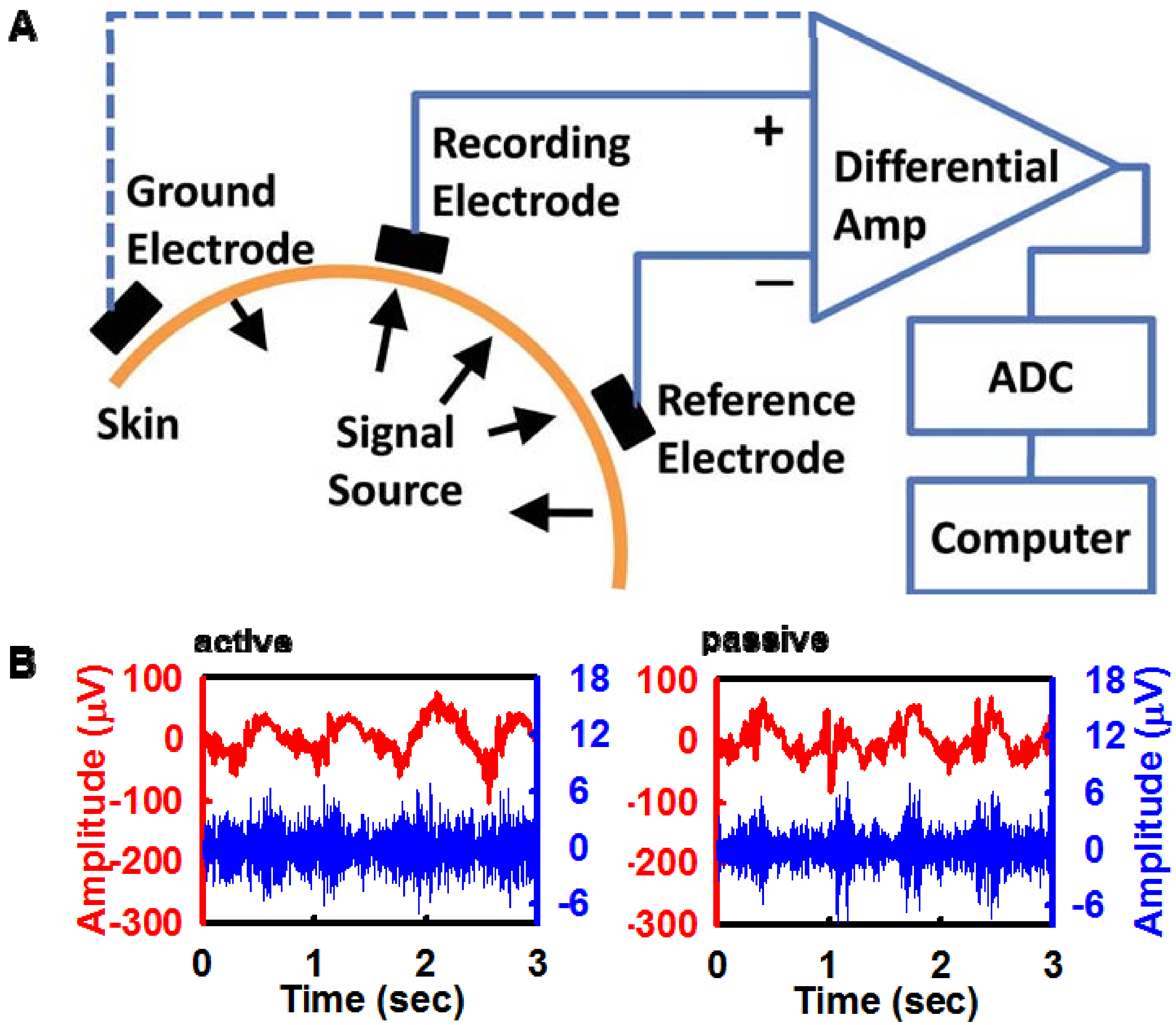

ECG

EMG leg

EMG leg

EEG forehead

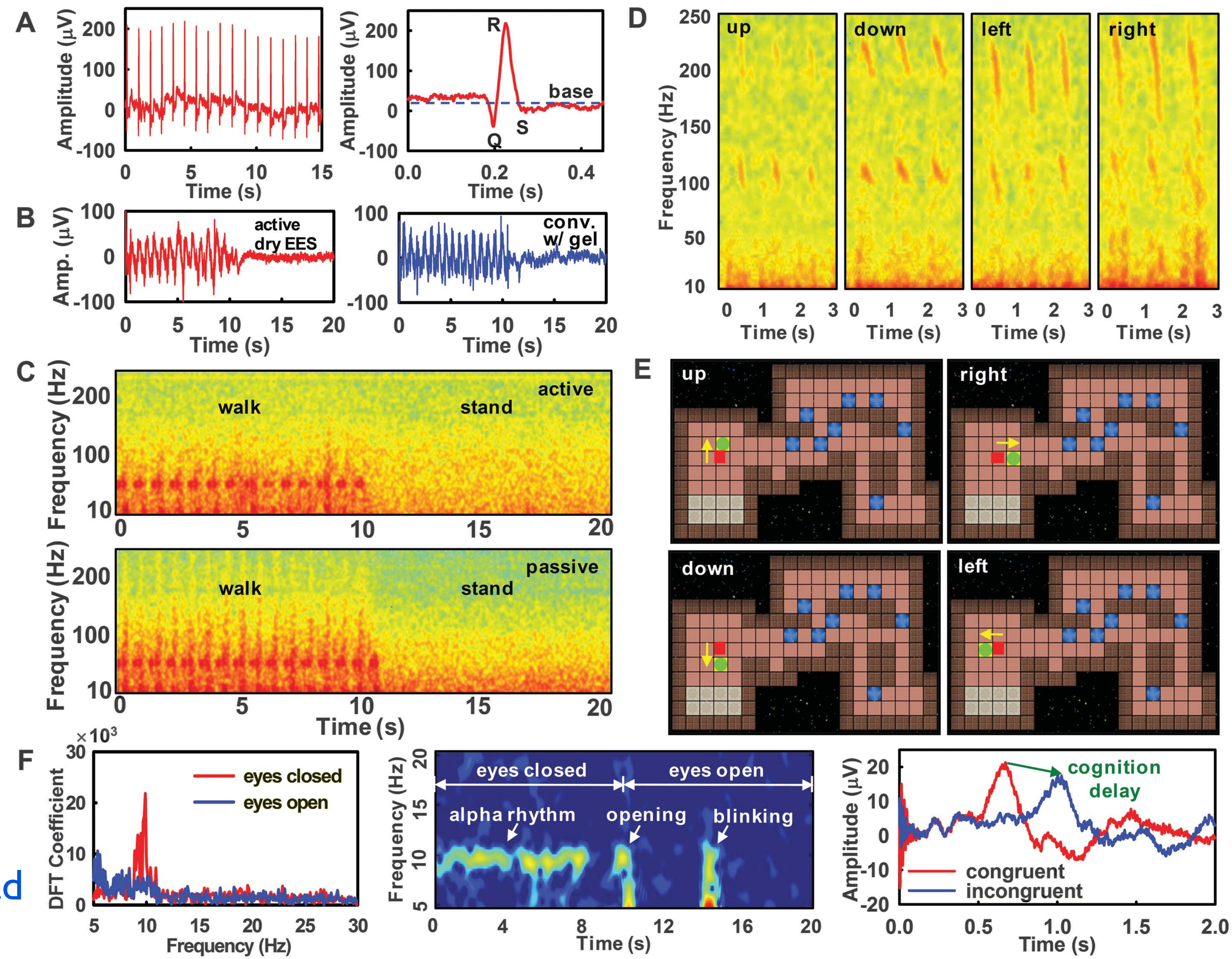

EMG throat

(>90%)

EMG-controlled game

EEG Stroop

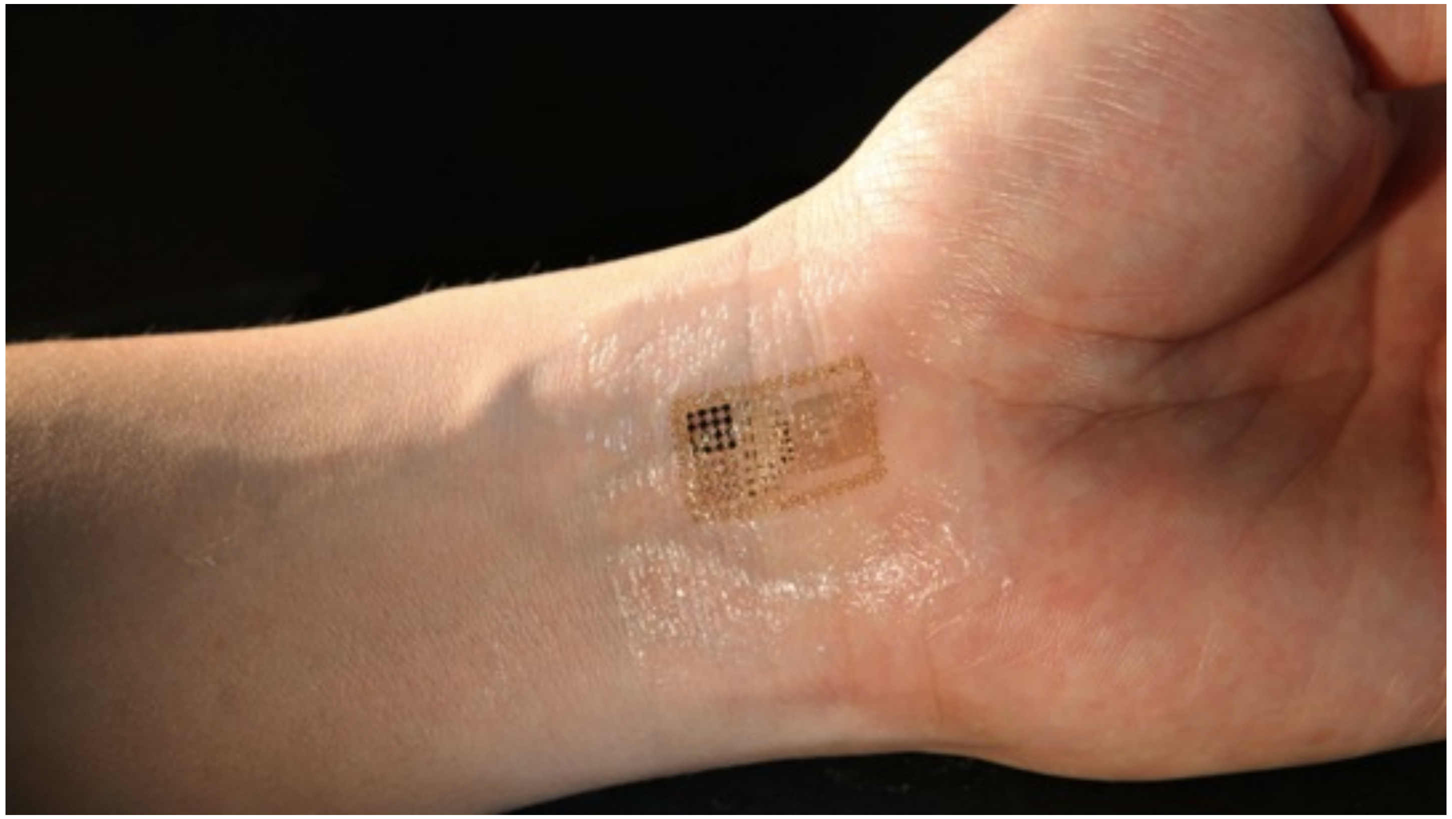

Demos